NASA Technical Memorandum 106520

# A New Flux-Conserving Numerical Scheme for the Steady, Incompressible Navier-Stokes Equations

James R. Scott
*Lewis Research Center*
*Cleveland, Ohio*

April 1994



NASA

# A New Flux-Conserving Numerical Scheme for the Steady, Incompressible Navier-Stokes Equations

James R. Scott
NASA Lewis Research Center
Cleveland, Ohio

## Abstract

This paper is concerned with the further development of a new numerical method, the space-time solution element (STS) method, for solving conservation laws. The present work focuses on the two-dimensional, steady, incompressible Navier-Stokes equations. Using first an integral approach, and then a differential approach, the discrete flux conservation equations presented in a recent paper are rederived. Here (i) a simpler method for determining the flux expressions at cell interfaces is given; (ii) a systematic and rigorous derivation of the conditions used to simulate the differential form of the governing conservation law(s) is provided; (iii) necessary and sufficient conditions for a discrete approximation to satisfy a conservation law in $E_2$ are derived; and (iv) an estimate of the local truncation error is given.

A specific scheme is then constructed for the solution of the thin airfoil boundary layer problem. Numerical results are presented which demonstrate the ability of the scheme to accurately resolve the developing boundary layer and wake regions using grids which are much coarser than those employed by other numerical methods. It is shown that ten cells in the cross-stream direction are sufficient to accurately resolve the developing airfoil boundary layer.

# A New Flux-Conserving Numerical Scheme for the Steady, Incompressible Navier-Stokes Equations

## I. Introduction

This paper is concerned with the further development of a new numerical method* for solving conservation laws.[1-4] The differences between the current method and the traditional finite-difference, finite-volume, finite-element, and spectral methods have been previously described.[1-4] The key differences may be summarized as follows: the current method (i) provides for a unified treatment of space and time; (ii) represents the local discrete solution through a Taylor series approximation that identically satisfies both the integral and differential forms of the governing conservation law(s); (iii) balances fluxes at cell interfaces as an integral part of the numerical formulation; and (iv) evaluates fluxes at cell boundaries using exact functional expressions (to the order of accuracy of the local expansions).

Specific numerical schemes[1-4] based on (i) – (iv) above have demonstrated the following properties: First, flux conservation is satisfied both locally and globally. Second, high accuracy is achieved without coupling the solution across numerous cells or grid points. Third, cells communicate only with their immediate neighbors, in much the same way that discrete regions of a real fluid interact. Fourth, the discrete dependent variables and their derivatives are all treated in a unified and consistent manner. Finally, the schemes themselves are conceptually simple and lend themselves to straightforward implementation.

In this paper, we are concerned with the continued development of a new flux-conserving numerical scheme for the steady Navier-Stokes equations.[3] Previous results have demonstrated the ability of this scheme to accurately resolve internal boundary layer flows on coarse, uniformly-spaced grids.

One purpose of this paper is to extend the internal scheme presented in [3] to external flow fields. The specific application that we consider is incompressible, laminar flow past a thin airfoil. In spite of the significant differences between external and internal flows, the scheme we propose here is a straightforward extension of the previously presented internal flow scheme. Through comparisons with the Blasius solution, we show that the thin airfoil boundary layer can be accurately resolved on sparse, coarsely-spaced grids.

Another purpose of the present work is to further illumine the flux conservation scheme presented in [3]. For simplicity, we concentrate in this paper on the incompressible Navier-Stokes equations. Using first an integral approach, and then a differential approach, we rederive the discrete flux conservation equations. Here we (i) present a simpler method for determining the flux expressions at cell interfaces; (ii) provide a systematic and rigorous derivation of the conditions used to simulate the differential form of the governing conservation law(s); (iii) derive necessary and sufficient conditions for a discrete approximation

*The Space-Time Solution Element (STS) Method, also called The Method of Space-Time Conservation Element and Solution Element

to satisfy a conservation law in $E_2$; and (iv) provide an estimate of the local truncation error.

In the next section, we derive the discrete flux conservation equations for the incompressible Navier-Stokes equations. We then construct a specific scheme for the solution of the thin airfoil boundary layer problem, and conclude with a discussion of numerical results.

## II. Numerical Formulation

### A. Conservation Laws for the Navier-Stokes Equations

We consider the two-dimensional, steady, incompressible Navier-Stokes equations in dimensionless form. We assume that the viscocity $\mu$ is constant, and denote the density by $\rho$ and the Reynolds number by $Re_L$, where $Re_L = \frac{\rho U_\infty L}{\mu}$. The parameters $L$ and $U_\infty$ refer to some reference length and velocity, respectively.

Let $x$ and $y$ denote the horizontal and vertical coordinates, respectively, of a two-dimensional Euclidean space $E_2$. Denoting the horizontal velocity component by $u$, the vertical velocity component by $v$, and the static pressure by $p$, the governing equations for the conservation of mass and momentum may be written in Cartesian coordinates as[5]

$$\frac{\partial u}{\partial x} + \frac{\partial v}{\partial y} = 0 \tag{2.1}$$

$$\frac{\partial}{\partial x}(u^2 + p - \tau_{xx}) + \frac{\partial}{\partial y}(u\,v - \tau_{xy}) = 0 \tag{2.2}$$

$$\frac{\partial}{\partial x}(u\,v - \tau_{xy}) + \frac{\partial}{\partial y}(v^2 + p - \tau_{yy}) = 0 \tag{2.3}$$

where

$$\tau_{xx} = \frac{2}{3Re_L}(2\frac{\partial u}{\partial x} - \frac{\partial v}{\partial y}) \tag{2.4}$$

$$\tau_{xy} = \frac{1}{Re_L}(\frac{\partial u}{\partial y} + \frac{\partial v}{\partial x}) \tag{2.5}$$

$$\tau_{yy} = \frac{2}{3Re_L}(2\frac{\partial v}{\partial y} - \frac{\partial u}{\partial x}) \tag{2.6}$$

(Although $\frac{\partial v}{\partial y}$ or $\frac{\partial u}{\partial x}$ may be eliminated from $\tau_{xx}$ and $\tau_{yy}$ using (2.1), we retain both terms here to be consistent with the compressible formulation presented in [3].)

By applying the divergence theorem to equations 2.1 - 2.3, they may be written in integral form as

$$\oint_{S(V)} \vec{h}_M \cdot \overrightarrow{ds} = 0 \tag{2.7}$$

$$\oint_{S(V)} \vec{h}_{XM} \cdot \overrightarrow{ds} = 0 \tag{2.8}$$

$$\oint_{S(V)} \vec{h}_{YM} \cdot \overrightarrow{ds} = 0 \tag{2.9}$$

where $S(V)$ is the boundary of an arbitrary region $V$ in $E_2$, and $\overrightarrow{ds}$ is equal to $d\sigma\,\vec{n}$, where $\vec{n}$ is the outward unit normal to $S(V)$ and $d\sigma$ is the length of a surface element of $S(V)$. The flux current density vectors, $\vec{h}_M$, $\vec{h}_{XM}$, and $\vec{h}_{YM}$, corresponding to the conservation of mass, x-momentum, and y-momentum, respectively, are given by

$$\vec{h}_M \stackrel{def}{=} (u, v) \tag{2.10}$$

$$\vec{h}_{XM} \stackrel{def}{=} (u^2 + p - \tau_{xx}, uv - \tau_{xy}) \tag{2.11}$$

$$\vec{h}_{YM} \stackrel{def}{=} (uv - \tau_{xy},\ v^2 + p - \tau_{yy}). \tag{2.12}$$

Equations 2.7 – 2.9 thus express physical conservation laws for the conservation of mass and momentum in an arbritrary region $V$ of $E_2$.

## B. Discrete Flux Conservation Equations – Integral Formulation

Let $E_2$ be discretized by a mesh with nonoverlapping rectangular regions. We assume constant spacing $\Delta x$ and $\Delta y$ in the $x$ and $y$ directions, respectively. (See Figure 1.) Each of the rectangular regions in the mesh will be referred to as both a conservation element and a solution element. A conservation element is a discrete region in $E_2$ over which the discrete analogue of the integral conservation laws (2.7) - (2.9) will be imposed. A solution element is a discrete region in $E_2$ in which a local Taylor series expansion is employed to represent the physical solution. In general, they need not refer to the same discrete region (See [2] or [4]). A conservation element will be denoted by $CE(i,j)$ and a solution element by $SE(i,j)$. The boundary of a conservation element will be denoted by $S(CE(i,j))$, and the cell center by $(x_i, y_j)$.

We then assume that the $u$ and $v$ velocity components and the static pressure $p$ can each be represented locally on a solution element by a two-dimensional Taylor series expansion about the cell center $(x_i, y_j)$ as follows:

$$\underset{\sim}{u}(x,y;i,j) \stackrel{def}{=} u_{0,0} + u_{1,0}(x-x_i) + u_{0,1}(y-y_j) + u_{2,0}(x-x_i)^2 + u_{1,1}(x-x_i)(y-y_j) + u_{0,2}(y-y_j)^2 \tag{2.13}$$

$$\underset{\sim}{v}(x,y;i,j) \stackrel{def}{=} v_{0,0} + v_{1,0}(x-x_i) + v_{0,1}(y-y_j) + v_{2,0}(x-x_i)^2 + v_{1,1}(x-x_i)(y-y_j) + v_{0,2}(y-y_j)^2 \tag{2.14}$$

$$\underset{\sim}{p}(x,y;i,j) \stackrel{def}{=} p_{0,0} + p_{1,0}(x-x_i) + p_{0,1}(y-y_j) + p_{2,0}(x-x_i)^2 + p_{1,1}(x-x_i)(y-y_j) + p_{0,2}(y-y_j)^2. \tag{2.15}$$

For clarity, the $i,j$ subscripts have been omitted from the coefficients in the Taylor series expansions. These coefficients are the unknowns to be solved for.

The Taylor series coefficients are related to the derivatives of the discrete dependent variables at the cell center by

$$u_{0,0} = \underset{\sim}{u} \tag{2.16}$$

$$u_{1,0} = \partial \underset{\sim}{u}/\partial x \tag{2.17}$$

$$u_{0,1} = \partial \underset{\sim}{u}/\partial y \tag{2.18}$$

$$u_{2,0} = \frac{1}{2}\,\partial^2 \underset{\sim}{u}/\partial x^2 \tag{2.19}$$

$$u_{1,1} = \partial^2 \underset{\sim}{u}/\partial x \partial y \tag{2.20}$$

$$u_{0,2} = \frac{1}{2}\,\partial^2 \underset{\sim}{u}/\partial y^2, \tag{2.21}$$

and similarly for $\underset{\sim}{v}$ and $\underset{\sim}{p}$.

The discrete analogue to equations 2.7 - 2.9 in $E_2$ is then given by

$$\oint_{S(CE(i,j))} \underset{\sim}{\vec{h}}_M \cdot \vec{ds} = 0 \tag{2.22}$$

$$\oint_{S(CE(i,j))} \vec{\underset{\sim}{h}}_{XM} \cdot \overrightarrow{ds} = 0 \tag{2.23}$$

$$\oint_{S(CE(i,j))} \vec{\underset{\sim}{h}}_{YM} \cdot \overrightarrow{ds} = 0 \tag{2.24}$$

where

$$\vec{\underset{\sim}{h}}_{M} \overset{def}{=} (\underset{\sim}{u}, \underset{\sim}{v}) \tag{2.25}$$

$$\vec{\underset{\sim}{h}}_{XM} \overset{def}{=} (\underset{\sim}{u}^2 + \underset{\sim}{p} - \underset{\sim}{\tau}_{xx}, \underset{\sim}{u}\,\underset{\sim}{v} - \underset{\sim}{\tau}_{xy}) \tag{2.26}$$

$$\vec{\underset{\sim}{h}}_{YM} \overset{def}{=} (\underset{\sim}{u}\,\underset{\sim}{v} - \underset{\sim}{\tau}_{xy}, \underset{\sim}{v}^2 + \underset{\sim}{p} - \underset{\sim}{\tau}_{yy}) \tag{2.27}$$

and

$$\underset{\sim}{\tau}_{xx} = \frac{2}{3Re_L}(2\,\partial \underset{\sim}{u}/\partial x - \partial \underset{\sim}{v}/\partial y) \tag{2.28}$$

$$\underset{\sim}{\tau}_{xy} = \frac{1}{Re_L}(\partial \underset{\sim}{u}/\partial y + \partial \underset{\sim}{v}/\partial x) \tag{2.29}$$

$$\underset{\sim}{\tau}_{yy} = \frac{2}{3Re_L}(2\,\partial \underset{\sim}{v}/\partial y - \partial \underset{\sim}{u}/\partial x). \tag{2.30}$$

Equations 2.22 – 2.24 are a coupled system of integral conservation laws in which the fluxes $\vec{\underset{\sim}{h}}_{M} \cdot \overrightarrow{ds}$, $\vec{\underset{\sim}{h}}_{XM} \cdot \overrightarrow{ds}$, and $\vec{\underset{\sim}{h}}_{YM} \cdot \overrightarrow{ds}$ are conserved by way of the discrete variables $\underset{\sim}{u}, \underset{\sim}{v}$ and $\underset{\sim}{p}$. Each equation takes the form

$$\oint_{S(CE(i,j))} \vec{\underset{\sim}{h}} \cdot \overrightarrow{ds} = 0, \tag{2.31}$$

where the second-order expansion $\vec{\underset{\sim}{h}}$ is a function of $\underset{\sim}{u}$, $\underset{\sim}{v}$ and $\underset{\sim}{p}$. Since the form of the integrals in (2.22) – (2.24) are identical, the integrations can be carried out by way of equation 2.31, where

$$\vec{\underset{\sim}{h}} \overset{def}{=} (\underset{\sim}{h}^x, \underset{\sim}{h}^y) \tag{2.32}$$

and

$$\underset{\sim}{h}^x(x,y;i,j) \stackrel{def}{=} h^x_{0,0} + h^x_{1,0}(x-x_i) + h^x_{0,1}(y-y_j) + h^x_{2,0}(x-x_i)^2 + h^x_{1,1}(x-x_i)(y-y_j) + h^x_{0,2}(y-y_j)^2 \tag{2.33}$$

$$\underset{\sim}{h}^y(x,y;i,j) \stackrel{def}{=} h^y_{0,0} + h^y_{1,0}(x-x_i) + h^y_{0,1}(y-y_j) + h^y_{2,0}(x-x_i)^2 + h^y_{1,1}(x-x_i)(y-y_j) + h^y_{0,2}(y-y_j)^2. \tag{2.34}$$

It is understood that each of the coefficients in (2.33) and (2.34) are functions of the discrete variables $u_{0,0}$, $v_{0,0}$, $p_{0,0}$, $u_{1,0}$, $v_{1,0}$, $p_{1,0}$, etc.. For example, when $\vec{\underset{\sim}{h}}$ corresponds to $\vec{\underset{\sim}{h}}_{XM}$, the term $h^x_{0,0}$ corresponds to the constant term of the expression $\underset{\sim}{u}^2 + \underset{\sim}{p} - \underset{\sim}{\tau}_{xx}$, and similarly for the other terms. Once the results are obtained in terms of $\vec{\underset{\sim}{h}}$, it is a simple matter to obtain the corresponding results for $\vec{\underset{\sim}{h}}_M$, $\vec{\underset{\sim}{h}}_{XM}$, and $\vec{\underset{\sim}{h}}_{YM}$ by way of equations 2.25 – 2.27.

The boundary $S(CE(i,j))$ of each conservation element is a simple closed curve in $E_2$. Consequently, the surface integration required in equation 2.31 can be converted into a line integration form.[1] With $\overrightarrow{ds} = d\sigma\,\vec{n}$, where $\vec{n}$ is the outward unit normal to $S(CE(i,j))$ and $d\sigma$ is the length of a surface element in $E_2$, we have

$$\overrightarrow{ds} \stackrel{def}{=} dy\,\vec{i} - dx\,\vec{j}, \tag{2.35}$$

and

$$\vec{\underset{\sim}{h}} \cdot \overrightarrow{ds} = -\underset{\sim}{h}^y\,dx + \underset{\sim}{h}^x\,dy = \vec{\underset{\sim}{g}} \cdot \vec{dr} \tag{2.36}$$

where

$$\vec{\underset{\sim}{g}} \stackrel{def}{=} (-\underset{\sim}{h}^y, \underset{\sim}{h}^x) \tag{2.37}$$

and

$$\vec{dr} \stackrel{def}{=} dx\,\vec{i} + dy\,\vec{j}. \tag{2.38}$$

The line integration is taken to be positive in the counterclockwise sense. If we denote the vertices of an arbritrary conservation element $CE(i,j)$ by $P$, $Q$, $R$, and $S$ as shown in Figure 2, we have

$$\oint_{S(CE(i,j))} \vec{\underset{\sim}{h}} \cdot \overrightarrow{ds} = \oint_{PQRS_{i,j}} \vec{\underset{\sim}{g}} \cdot \vec{dr}$$

$$\stackrel{def}{=} \left[ J(\overline{PQ}) + J(\overline{QR}) + J(\overline{RS}) + J(\overline{SP}) \right]_{i,j}. \tag{2.39}$$

$[J(\overline{PQ})]_{i,j}$ denotes the flux of $\vec{\underset{\sim}{h}}$ through the line segment $\overline{PQ}_{i,j}$, and similarly for $J(\overline{QR})$, $J(\overline{RS})$, and $J(\overline{SP})$. We then have (omitting $i,j$ subscripts)

$$\begin{aligned} J(\overline{PQ}) &\stackrel{def}{=} \int_P^Q -\underset{\sim}{h}^y\,dx + \underset{\sim}{h}^x\,dy \\ &= \int_{x_i+\frac{\Delta x}{2}}^{x_i-\frac{\Delta x}{2}} -\underset{\sim}{h}^y\,dx + \underset{\sim}{h}^x\,dy \qquad (2.40) \\ &= \int_{x_i-\frac{\Delta x}{2}}^{x_i+\frac{\Delta x}{2}} \underset{\sim}{h}^y\,dx \qquad \text{with} \quad y = y_j + \frac{\Delta y}{2}. \end{aligned}$$

Similarly,

$$J(\overline{QR}) \stackrel{def}{=} -\int_{y_j-\frac{\Delta y}{2}}^{y_j+\frac{\Delta y}{2}} \underset{\sim}{h}^x\,dy \qquad \text{with} \quad x = x_i - \frac{\Delta x}{2} \qquad (2.41)$$

$$J(\overline{RS}) \stackrel{def}{=} -\int_{x_i-\frac{\Delta x}{2}}^{x_i+\frac{\Delta x}{2}} \underset{\sim}{h}^y\,dx \qquad \text{with} \quad y = y_j - \frac{\Delta y}{2} \qquad (2.42)$$

$$J(\overline{SP}) \stackrel{def}{=} \int_{y_j-\frac{\Delta y}{2}}^{y_j+\frac{\Delta y}{2}} \underset{\sim}{h}^x\,dy \qquad \text{with} \quad x = x_i + \frac{\Delta x}{2}. \qquad (2.43)$$

Carrying out the line integrations in equations 2.40 - 2.43, one easily obtains

$$J(\overline{PQ}) = \frac{\Delta x^3}{12} h^y_{2,0} + \Delta x \left[\frac{\Delta y^2}{4} h^y_{0,2} + \frac{\Delta y}{2} h^y_{0,1} + h^y_{0,0}\right] \qquad (2.44)$$

$$J(\overline{QR}) = -\frac{\Delta y^3}{12} h^x_{0,2} - \Delta y \left[\frac{\Delta x^2}{4} h^x_{2,0} - \frac{\Delta x}{2} h^x_{1,0} + h^x_{0,0}\right] \qquad (2.45)$$

$$J(\overline{RS}) = -\frac{\Delta x^3}{12} h^y_{2,0} - \Delta x \left[\frac{\Delta y^2}{4} h^y_{0,2} - \frac{\Delta y}{2} h^y_{0,1} + h^y_{0,0}\right] \qquad (2.46)$$

$$J(\overline{SP}) = \frac{\Delta y^3}{12} h^x_{0,2} + \Delta y \left[\frac{\Delta x^2}{4} h^x_{2,0} + \frac{\Delta x}{2} h^x_{1,0} + h^x_{0,0}\right]. \qquad (2.47)$$

By virtue of equations 2.31 and 2.39 we require that

$$J(\overline{PQ}) + J(\overline{QR}) + J(\overline{RS}) + J(\overline{SP}) \equiv 0. \tag{2.48}$$

Thus, we obtain the *flux conservation constraint*

$$h^x_{1,0} + h^y_{0,1} = 0. \tag{2.49}$$

Imposing this condition, we obtain the following expressions for the normalized flux of $\vec{h}$ across the boundaries of $CE(i,j)$:

$$\frac{J(\overline{PQ})}{\Delta x} = \frac{\Delta x^2}{12} h^y_{2,0} + \frac{\Delta y^2}{4} h^y_{0,2} - \frac{\Delta y}{2} h^x_{1,0} + h^y_{0,0} \tag{2.50}$$

$$-\frac{J(\overline{QR})}{\Delta y} = \frac{\Delta y^2}{12} h^x_{0,2} + \frac{\Delta x^2}{4} h^x_{2,0} - \frac{\Delta x}{2} h^x_{1,0} + h^x_{0,0} \tag{2.51}$$

$$-\frac{J(\overline{RS})}{\Delta x} = \frac{\Delta x^2}{12} h^y_{2,0} + \frac{\Delta y^2}{4} h^y_{0,2} + \frac{\Delta y}{2} h^x_{1,0} + h^y_{0,0} \tag{2.52}$$

$$\frac{J(\overline{SP})}{\Delta y} = \frac{\Delta y^2}{12} h^x_{0,2} + \frac{\Delta x^2}{4} h^x_{2,0} + \frac{\Delta x}{2} h^x_{1,0} + h^x_{0,0}. \tag{2.53}$$

Equations 2.50 – 2.53 are a third-order-accurate representation of the flux through the boundaries of $CE(i,j)$.

The flux expressions above may now be expressed in terms of the discrete dependent variables of the Navier-Stokes equations by way of equations 2.25 – 2.27. Corresponding to (2.25), we have

$$\vec{h} = \vec{h}_M \tag{2.54}$$

so that

$$h^x = u \tag{2.55a}$$

$$h^y = v \tag{2.55b}$$

and the mass flux conservation constraint corresponding to (2.49) is

$$u_{1,0} + v_{0,1} = 0. \tag{2.56}$$

The normalized flux expressions for $\vec{\underset{\sim}{h}}_M$ are

$$\frac{J(\overline{PQ})_M}{\Delta x} = \frac{\Delta x^2}{12} v_{2,0} + \frac{\Delta y^2}{4} v_{0,2} - \frac{\Delta y}{2} u_{1,0} + v_{0,0} \tag{2.57}$$

$$-\frac{J(\overline{QR})_M}{\Delta y} = \frac{\Delta y^2}{12} u_{0,2} + \frac{\Delta x^2}{4} u_{2,0} - \frac{\Delta x}{2} u_{1,0} + u_{0,0} \tag{2.58}$$

$$-\frac{J(\overline{RS})_M}{\Delta x} = \frac{\Delta x^2}{12} v_{2,0} + \frac{\Delta y^2}{4} v_{0,2} + \frac{\Delta y}{2} u_{1,0} + v_{0,0} \tag{2.59}$$

$$\frac{J(\overline{SP})_M}{\Delta y} = \frac{\Delta y^2}{12} u_{0,2} + \frac{\Delta x^2}{4} u_{2,0} + \frac{\Delta x}{2} u_{1,0} + u_{0,0}. \tag{2.60}$$

Corresponding to (2.26), we have

$$\vec{\underset{\sim}{h}} = \vec{\underset{\sim}{h}}_{XM} \tag{2.61}$$

so that

$$\underset{\sim}{h}^x = \underset{\sim}{u}^2 + \underset{\sim}{p} - \underset{\sim}{\tau}_{xx} \tag{2.62a}$$

$$\underset{\sim}{h}^y = \underset{\sim}{u}\,\underset{\sim}{v} - \underset{\sim}{\tau}_{xy}. \tag{2.62b}$$

The x-momentum flux conservation constraint corresponding to (2.49) is

$$u_{1,0}\,u_{0,0} + u_{0,1}\,v_{0,0} + p_{1,0} - \frac{1}{Re_L}[(2\,u_{0,2} + v_{1,1}) + \frac{2}{3}(4\,u_{2,0} - v_{1,1})] = 0, \tag{2.63}$$

and the normalized flux expressions for $\vec{\underset{\sim}{h}}_{XM}$ are

$$\frac{J(\overline{PQ})_{XM}}{\Delta x} = \tag{2.64}$$

$$\frac{\Delta x^2}{12}(u_{2,0}\,v_{0,0} + v_{2,0}\,u_{0,0} + u_{1,0}\,v_{1,0}) + \frac{\Delta y^2}{4}(u_{0,2}\,v_{0,0} + v_{0,2}\,u_{0,0} + u_{0,1}\,v_{0,1})$$

$$+ \frac{\Delta y}{2}\left[v_{0,0}\,u_{0,1} - u_{0,0}\,u_{1,0} - \frac{1}{Re_L}(2\,u_{0,2} + v_{1,1})\right] - \frac{1}{Re_L}(u_{0,1} + v_{1,0}) + u_{0,0}\,v_{0,0}$$

$$-\frac{J(\overline{QR})_{xM}}{\Delta y} = \tag{2.65}$$

$$\frac{\Delta y^2}{12}(2\,u_{0,2}\,u_{0,0} + u_{0,1}^2 + p_{0,2}) + \frac{\Delta x^2}{4}(2\,u_{2,0}\,u_{0,0} + u_{1,0}^2 + p_{2,0})$$

$$+\frac{\Delta x}{2}\left[v_{0,0}\,u_{0,1} - u_{0,0}\,u_{1,0} - \frac{1}{Re_L}(2\,u_{0,2} + v_{1,1})\right] + p_{0,0} - \frac{2}{3Re_L}(2\,u_{1,0} - v_{0,1}) + u_{0,0}^2$$

$$-\frac{J(\overline{RS})_{xM}}{\Delta x} = \tag{2.66}$$

$$\frac{\Delta x^2}{12}(u_{2,0}\,v_{0,0} + v_{2,0}\,u_{0,0} + u_{1,0}\,v_{1,0}) + \frac{\Delta y^2}{4}(u_{0,2}\,v_{0,0} + v_{0,2}\,u_{0,0} + u_{0,1}\,v_{0,1})$$

$$-\frac{\Delta y}{2}\left[v_{0,0}\,u_{0,1} - u_{0,0}\,u_{1,0} - \frac{1}{Re_L}(2\,u_{0,2} + v_{1,1})\right] - \frac{1}{Re_L}(u_{0,1} + v_{1,0}) + u_{0,0}\,v_{0,0}$$

$$\frac{J(\overline{SP})_{xM}}{\Delta y} = \tag{2.67}$$

$$\frac{\Delta y^2}{12}(2\,u_{0,2}\,u_{0,0} + u_{0,1}^2 + p_{0,2}) + \frac{\Delta x^2}{4}(2\,u_{2,0}\,u_{0,0} + u_{1,0}^2 + p_{2,0})$$

$$-\frac{\Delta x}{2}\left[v_{0,0}\,u_{0,1} - u_{0,0}\,u_{1,0} - \frac{1}{Re_L}(2\,u_{0,2} + v_{1,1})\right] + p_{0,0} - \frac{2}{3Re_L}(2\,u_{1,0} - v_{0,1}) + u_{0,0}^2.$$

(In applying (2.50) – (2.53) to the x-momentum equation, we have replaced $h^x_{1,0}$ with $-h^y_{0,1}$ because it gives a simpler expression.)

Corresponding to (2.27), we have

$$\vec{\underset{\sim}{h}} = \vec{\underset{\sim}{h}}_{YM} \tag{2.68}$$

with

$$\underset{\sim}{h}^x = \underset{\sim}{u}\,\underset{\sim}{v} - \underset{\sim}{\tau}_{xy} \tag{2.69a}$$

$$\underset{\sim}{h}^y = \underset{\sim}{v}^2 + \underset{\sim}{p} - \underset{\sim}{\tau}_{yy}. \tag{2.69b}$$

The y-momentum flux conservation constraint is

$$v_{1,0}\,u_{0,0} + v_{0,1}\,v_{0,0} + p_{0,1} - \frac{1}{Re_L}[(2\,v_{2,0} + u_{1,1}) + \frac{2}{3}(4\,v_{0,2} - u_{1,1})] = 0, \tag{2.70}$$

and the normalized flux expressions for $\vec{h}_{YM}$ are

$$\frac{J(\overline{PQ})_{YM}}{\Delta x} = \tag{2.71}$$

$$\frac{\Delta x^2}{12}(2\,v_{2,0}\,v_{0,0} + v_{1,0}^2 + p_{2,0}) + \frac{\Delta y^2}{4}(2\,v_{0,2}\,v_{0,0} + v_{0,1}^2 + p_{0,2})$$

$$- \frac{\Delta y}{2}\left[u_{0,0}\,v_{1,0} + v_{0,0}\,u_{1,0} - \frac{1}{Re_L}(2\,v_{2,0} + u_{1,1})\right] + p_{0,0} - \frac{2}{3Re_L}(2\,v_{0,1} - u_{1,0}) + v_{0,0}^2$$

$$-\frac{J(\overline{QR})_{YM}}{\Delta y} = \tag{2.72}$$

$$\frac{\Delta y^2}{12}(v_{0,2}\,u_{0,0} + u_{0,2}\,v_{0,0} + v_{0,1}\,u_{0,1}) + \frac{\Delta x^2}{4}(v_{2,0}\,u_{0,0} + u_{2,0}\,v_{0,0} + v_{1,0}\,u_{1,0})$$

$$- \frac{\Delta x}{2}\left[u_{0,0}\,v_{1,0} + v_{0,0}\,u_{1,0} - \frac{1}{Re_L}(2\,v_{2,0} + u_{1,1})\right] - \frac{1}{Re_L}(u_{0,1} + v_{1,0}) + v_{0,0}\,u_{0,0}$$

$$-\frac{J(\overline{RS})_{YM}}{\Delta x} = \tag{2.73}$$

$$\frac{\Delta x^2}{12}(2\,v_{2,0}\,v_{0,0} + v_{1,0}^2 + p_{2,0}) + \frac{\Delta y^2}{4}(2\,v_{0,2}\,v_{0,0} + v_{0,1}^2 + p_{0,2})$$

$$+ \frac{\Delta y}{2}\left[u_{0,0}\,v_{1,0} + v_{0,0}\,u_{1,0} - \frac{1}{Re_L}(2\,v_{2,0} + u_{1,1})\right] + p_{0,0} - \frac{2}{3Re_L}(2\,v_{0,1} - u_{1,0}) + v_{0,0}^2$$

$$\frac{J(\overline{SP})_{YM}}{\Delta y} = \tag{2.74}$$

$$\frac{\Delta y^2}{12}(v_{0,2}\,u_{0,0} + u_{0,2}\,v_{0,0} + v_{0,1}\,u_{0,1}) + \frac{\Delta x^2}{4}(v_{2,0}\,u_{0,0} + u_{2,0}\,v_{0,0} + v_{1,0}\,u_{1,0})$$

$$+ \frac{\Delta x}{2}\left[u_{0,0}\,v_{1,0} + v_{0,0}\,u_{1,0} - \frac{1}{Re_L}(2\,v_{2,0} + u_{1,1})\right] - \frac{1}{Re_L}(u_{0,1} + v_{1,0}) + v_{0,0}\,u_{0,0}.$$

The following conditions are then satisfied on each conservation element:

$$J(\overline{PQ})_M + J(\overline{QR})_M + J(\overline{RS})_M + J(\overline{SP})_M \equiv 0 \tag{2.75}$$

$$J(\overline{PQ})_{XM} + J(\overline{QR})_{XM} + J(\overline{RS})_{XM} + J(\overline{SP})_{XM} \equiv 0 \tag{2.76a}$$

$$J(\overline{PQ})_{YM} + J(\overline{QR})_{YM} + J(\overline{RS})_{YM} + J(\overline{SP})_{YM} \equiv 0. \tag{2.76b}$$

Thus, the total mass and momentum flux out of each conservation element is exactly zero. Furthermore, the discrete variables $\underset{\sim}{u}$, $\underset{\sim}{v}$, and $\underset{\sim}{p}$ satisfy the Navier-Stokes equations in integral form.

The above formulation provides the framework through which local and global flux conservation is achieved. We may now turn our attention to the differential conservation laws (2.1) - (2.3).

### C. Discrete Flux Conservation Equations – Differential Formulation

We begin with a consideration of the general conservation law

$$\vec{\nabla} \cdot \vec{\mathcal{H}} = 0. \tag{2.77}$$

Let

$$\vec{h} = (h^x, h^y) \tag{2.78}$$

be defined and continuous on an open domain $\mathcal{D}$ of $E_2$. Suppose that the partial derivatives of $h^x$ and $h^y$ exist to all orders and are continuous on $\mathcal{D}$. Then, a necessary and sufficient condition for $\vec{h}$ to be a solution of (2.77) in $\mathcal{D}$ is that its partial derivatives satisfy

$$\frac{\partial^n h^x}{\partial x^{n-k}\,\partial y^k} + \frac{\partial^n h^y}{\partial x^{n-k-1}\,\partial y^{k+1}} = 0 \tag{2.79}$$

$$\text{for } n = 1, 2, 3, \ldots \text{ and } k = 0, 1, 2, \ldots, n-1.$$

For $n = 1$ this gives

$$\frac{\partial h^x}{\partial x} + \frac{\partial h^y}{\partial y} = 0 \tag{2.80}$$

and for $n = 2$

$$\frac{\partial^2 h^x}{\partial x^2} + \frac{\partial^2 h^y}{\partial x \partial y} = 0 \tag{2.81a}$$

$$\frac{\partial^2 h^x}{\partial x \partial y} + \frac{\partial^2 h^y}{\partial y^2} = 0. \tag{2.81b}$$

If $\vec{h}$ is a solution of (2.77), then (2.80) holds. Equation 2.79 follows by repeated differentiation of equation 2.80 with respect to $x$ and $y$. The general result can be established by induction.

Conversely, (2.80) shows that if $\vec{h}$ satisfies (2.79), then $\vec{h}$ is a solution of (2.77).

On the basis of the above, we state the following theorem:

*Theorem 2.1* Let $\vec{h} = (h^x, h^y)$ be defined and continuous on an open domain $\mathcal{D}$ of $E_2$, and let the partial derivatives of $h^x$ and $h^y$ exist to all orders and be continuous on $\mathcal{D}$. Then, $\vec{h}$ satisfies $\vec{\nabla} \cdot \vec{h} = 0$ throughout $\mathcal{D}$ if and only if its partial derivatives satisfy

$$\frac{\partial^n h^x}{\partial x^{n-k}\,\partial y^k}(x,y) + \frac{\partial^n h^y}{\partial x^{n-k-1}\,\partial y^{k+1}}(x,y) = 0$$
$$\text{for } n = 1,2,3,\ldots \text{ and } k = 0,1,2,\ldots,n-1,$$

for every $(x,y)$ in $\mathcal{D}$.

Now suppose that $\vec{h}$ is a solution of (2.77), and that $h^x$ and $h^y$ are also analytic throughout $\mathcal{D}$. Near any $(x_0, y_0)$ in $\mathcal{D}$, we have the uniformly convergent Taylor series expansions

$$h^x(x,y) = h^x(x_0,y_0) + \frac{\partial h^x}{\partial x}(x_0,y_0)(x-x_0) + \frac{\partial h^x}{\partial y}(x_0,y_0)(y-y_0) + \cdots$$
$$= \sum_{n=0}^{\infty}\sum_{k=0}^{n}\Big[\frac{\partial^n h^x}{\partial x^{n-k}\partial y^k}(x_0,y_0)\Big]\frac{(x-x_0)^{n-k}}{(n-k)!}\,\frac{(y-y_0)^k}{k!} \tag{2.82}$$

$$h^y(x,y) = h^y(x_0,y_0) + \frac{\partial h^y}{\partial x}(x_0,y_0)(x-x_0) + \frac{\partial h^y}{\partial y}(x_0,y_0)(y-y_0) + \cdots$$
$$= \sum_{n=0}^{\infty}\sum_{k=0}^{n}\Big[\frac{\partial^n h^y}{\partial x^{n-k}\partial y^k}(x_0,y_0)\Big]\frac{(x-x_0)^{n-k}}{(n-k)!}\,\frac{(y-y_0)^k}{k!} \tag{2.83}$$

$$\frac{\partial h^x}{\partial x} = \frac{\partial h^x}{\partial x}(x_0,y_0) + \frac{\partial^2 h^x}{\partial x^2}(x_0,y_0)(x-x_0) + \frac{\partial^2 h^x}{\partial y\partial x}(x_0,y_0)(y-y_0) + \cdots$$
$$= \sum_{n=1}^{\infty}\sum_{k=0}^{n-1}\Big[\frac{\partial^n h^x}{\partial x^{n-k}\partial y^k}(x_0,y_0)\Big]\frac{(x-x_0)^{n-k-1}}{(n-k-1)!}\,\frac{(y-y_0)^k}{k!} \tag{2.84}$$

$$\frac{\partial h^y}{\partial y} = \frac{\partial h^y}{\partial y}(x_0,y_0) + \frac{\partial^2 h^y}{\partial x\partial y}(x_0,y_0)(x-x_0) + \frac{\partial^2 h^y}{\partial y^2}(x_0,y_0)(y-y_0) + \cdots$$
$$= \sum_{n=1}^{\infty}\sum_{k=1}^{n}\Big[\frac{\partial^n h^y}{\partial x^{n-k}\partial y^k}(x_0,y_0)\Big]\frac{(x-x_0)^{n-k}}{(n-k)!}\,\frac{(y-y_0)^{(k-1)}}{(k-1)!}$$
$$= \sum_{n=1}^{\infty}\sum_{k=0}^{n-1}\Big[\frac{\partial^n h^y}{\partial x^{n-k-1}\partial y^{k+1}}(x_0,y_0)\Big]\frac{(x-x_0)^{n-k-1}}{(n-k-1)!}\,\frac{(y-y_0)^k}{k!} \tag{2.85}$$

where $\frac{\partial^0}{\partial x^0 \partial y^0} \stackrel{def}{=} 1$, $\frac{\partial^1}{\partial x^1 \partial y^0} \stackrel{def}{=} \frac{\partial}{\partial x}$, and $\frac{\partial^1}{\partial x^0 \partial y^1} \stackrel{def}{=} \frac{\partial}{\partial y}$.

We now examine the effect of truncating (2.82) and (2.83). Let

$$h_N^x(x,y) = \sum_{n=0}^{N} \sum_{k=0}^{n} \Big[ \frac{\partial^n h^x}{\partial x^{n-k} \partial y^k}(x_0, y_0) \Big] \frac{(x-x_0)^{n-k}}{(n-k)!} \frac{(y-y_0)^k}{k!} \tag{2.86}$$

and

$$h_N^y(x,y) = \sum_{n=0}^{N} \sum_{k=0}^{n} \Big[ \frac{\partial^n h^y}{\partial x^{n-k} \partial y^k}(x_0, y_0) \Big] \frac{(x-x_0)^{n-k}}{(n-k)!} \frac{(y-y_0)^k}{k!} \tag{2.87}$$

be the $N$th-order Taylor series expansions of $h^x$ and $h^y$, respectively. Then

$$h^x(x,y) - h_N^x(x,y) = \sum_{k=0}^{N+1} \Big[ \frac{\partial^{N+1} h^x}{\partial x^{N+1-k} \partial y^k}(x_1^*, y_1^*) \Big] \frac{(x-x_0)^{N+1-k}}{(N+1-k)!} \frac{(y-y_0)^k}{k!} \tag{2.88}$$

where $(x_1^*, y_1^*)$ is a point on the line segment between $(x_0, y_0)$ and $(x, y)$.[6] Similarly,

$$h^y(x,y) - h_N^y(x,y) = \sum_{k=0}^{N+1} \Big[ \frac{\partial^{N+1} h^y}{\partial x^{N+1-k} \partial y^k}(x_2^*, y_2^*) \Big] \frac{(x-x_0)^{N+1-k}}{(N+1-k)!} \frac{(y-y_0)^k}{k!}. \tag{2.89}$$

Let

$$\Big| \frac{\partial^{N+1} h^x}{\partial x^{N+1-k} \partial y^k} \Big| \leq M_{N+1,k}^x \quad \text{and} \quad \Big| \frac{\partial^{N+1} h^y}{\partial x^{N+1-k} \partial y^k} \Big| \leq M_{N+1,k}^y$$

in a neighborhood $N_0$ of $(x_0, y_0)$ for $k = 0, 1, ..., N+1$. If $\Delta x = (x - x_0)$ and $\Delta y = (y - y_0)$ where $(x, y)$ is any point in $N_0$, then

$$|h^x(x,y) - h_N^x(x,y)| \leq \sum_{k=0}^{N+1} M_{N+1,k}^x \frac{\Delta x^{N+1-k}}{(N+1-k)!} \frac{\Delta y^k}{k!} \tag{2.90}$$

and

$$|h^y(x,y) - h_N^y(x,y)| \leq \sum_{k=0}^{N+1} M_{N+1,k}^y \frac{\Delta x^{N+1-k}}{(N+1-k)!} \frac{\Delta y^k}{k!}. \tag{2.91}$$

Let $M_{N+1} = \sup\{M_{N+1,k}^x, M_{N+1,k}^y,\ k = 0, 1, ..., N+1\}$. Then we have the more conservative error estimates

$$|h^x(x,y) - h_N^x(x,y)| < \frac{M_{N+1}\,(N+2)\,[\max(\Delta x, \Delta y)]^{N+1}}{[(\frac{N+1}{2})!]^2} \tag{2.92}$$

and

$$|h^y(x,y) - h_N^y(x,y)| < \frac{M_{N+1}(N+2)[\max(\Delta x, \Delta y)]^{N+1}}{[(\frac{N+1}{2})!]^2}. \tag{2.93}$$

If $N$ is an even number, then $[(\frac{N+1}{2})!]^2$ is defined by

$$[(\frac{N+1}{2})!]^2 = (\frac{N}{2}+\frac{1}{2})!\,(\frac{N}{2}+\frac{1}{2})!$$

$$\stackrel{def}{=} (\frac{N}{2}+\frac{1}{2}-\frac{1}{2})!\,(\frac{N}{2}+\frac{1}{2}+\frac{1}{2})! = (\frac{N}{2})!\,(\frac{N+2}{2})!. \tag{2.94}$$

Equations 2.84 – 2.87 together with *Theorem 2.1* show clearly that the function $\vec{h}_N \stackrel{def}{=} (h_N^x, h_N^y)$ is a solution of the governing conservation law (2.77). Its order of accuracy is given by (2.92) - (2.93). It follows that a necessary condition for a local polynomial approximation $\underset{\sim}{\vec{h}}_n$ to be the Taylor series approximation $\vec{h}_n$ to $\vec{h}$ is that it be a solution of Equation 2.77.

To proceed further, we need to formalize the notions of "a local polynomial approximation" and "convergence."

*Definition 2.1* Let $(x_0, y_0)$ be a point in $E_2$, and let $\Delta x$ and $\Delta y$ be positive numbers. Let $N_{0\Delta x\Delta y} = \left\{(x,y) : |x-x_0| \le \frac{\Delta x}{2} \text{ and } |y-y_0| \le \frac{\Delta y}{2}\right\}$. Then, a local discrete polynomial approximation is a function $\underset{\sim}{\vec{h}}_N \stackrel{def}{=} (\underset{\sim}{h}^x_N, \underset{\sim}{h}^y_N)$ defined on $N_{0\Delta x\Delta y}$ by

$$\underset{\sim}{h}^x_N(x,y) = \sum_{n=0}^{N}\sum_{k=0}^{n} h^x_{n-k,k}(\Delta x, \Delta y)\,(x-x_0)^{n-k}\,(y-y_0)^k \tag{2.95}$$

$$\underset{\sim}{h}^y_N(x,y) = \sum_{n=0}^{N}\sum_{k=0}^{n} h^y_{n-k,k}(\Delta x, \Delta y)\,(x-x_0)^{n-k}\,(y-y_0)^k, \tag{2.96}$$

where $h^x_{n-k,k}$ and $h^y_{n-k,k}$ are functions of $\Delta x$ and $\Delta y$.

*Definition 2.2* A local discrete polynomial approximation $\underset{\sim}{\vec{h}}_N$ converges to order $K$ to the exact solution $\vec{h}$ of the conservation law $\vec{\nabla}\cdot\vec{\mathcal{H}} = 0$ as $\Delta x \to 0$, $\Delta y \to 0$ if and only if for any $\epsilon > 0$, there exist numbers $\delta_1 > 0$ and $\delta_2 > 0$ such that when $\Delta x < \delta_1$ and $\Delta y < \delta_2$,

$$\left|h^x_{n-k,k}(\Delta x, \Delta y) - \frac{\partial^n h^x}{\partial x^{n-k}\partial y^k}(x_0,y_0)\,\frac{1}{(n-k)!}\,\frac{1}{k!}\right| < \epsilon \tag{2.97}$$

$$\left|h^y_{n-k,k}(\Delta x, \Delta y) - \frac{\partial^n h^y}{\partial x^{n-k}\partial y^k}(x_0,y_0)\,\frac{1}{(n-k)!}\,\frac{1}{k!}\right| < \epsilon \tag{2.98}$$

for $n = 0, 1, ..., K$, and $k = 0, 1, ..., n$, and the remainder $\underset{\sim}{\vec{R}}_K = \underset{\sim}{\vec{h}}_N - \underset{\sim}{\vec{h}}_K \to \vec{0}$ as $\Delta x \to 0$, $\Delta y \to 0$.

We may now state and prove the two following important theorems.

*Theorem 2.2* Let $\epsilon$ be any positive number, and let $0 \leq K \leq N$. If $\vec{\tilde{h}}_N(\Delta x, \Delta y)$ converges to order $K$ to the exact solution $\vec{h}$ of the conservation law $\vec{\nabla} \cdot \vec{\mathcal{H}} = 0$ as $\Delta x \to 0$, $\Delta y \to 0$, then for all sufficiently small $\Delta x$ and $\Delta y$,

$$\|\vec{h} - \vec{\tilde{h}}_N(\Delta x, \Delta y)\|_\infty < \epsilon.$$

*Proof:*

We have

$$\vec{h} - \vec{\tilde{h}}_N = \vec{h} - \vec{h}_N + \vec{h}_N - \vec{\tilde{h}}_N \tag{2.2a}$$

$$\Rightarrow \quad \|\vec{h} - \vec{\tilde{h}}_N\|_\infty \leq \|\vec{h} - \vec{h}_N\|_\infty + \|\vec{h}_N - \vec{\tilde{h}}_N\|_\infty \tag{2.2b}$$

$$\Rightarrow \quad \|\vec{h} - \vec{\tilde{h}}_N\|_\infty \leq \|\vec{h} - \vec{h}_N\|_\infty + \|\vec{h}_K - \vec{\tilde{h}}_K\|_\infty + \|\vec{R}_K - \vec{\tilde{R}}_K\|_\infty \tag{2.2c}$$

where $\vec{R}_K = \vec{h}_N - \vec{h}_K$ and $\vec{\tilde{R}}_K = \vec{\tilde{h}}_N - \vec{\tilde{h}}_K$. The first two terms on the right hand side of *(2.2c)* are each less than $\frac{\epsilon}{3}$ for sufficiently small $\Delta x$ and $\Delta y$, and the third term is a polynomial whose lowest order term is of degree $K+1$. Since the coefficients of $\vec{R}_K$ are fixed, and $\vec{\tilde{R}}_K \to \vec{0}$, the third term is also less than $\frac{\epsilon}{3}$ for sufficiently small $\Delta x$ and $\Delta y$, and the theorem follows.

*Theorem 2.3* Let $\epsilon$ be any positive number, and let $1 \leq K \leq N$. If $\vec{\tilde{h}}_N(\Delta x, \Delta y)$ converges to order $K$ to the exact solution $\vec{h}$ of the conservation law $\vec{\nabla} \cdot \vec{\mathcal{H}} = 0$ as $\Delta x \to 0$, $\Delta y \to 0$, then for all sufficiently small $\Delta x$ and $\Delta y$,

$$(n-k)\, h^x_{n-k,k}(\Delta x, \Delta y) + (k+1)\, h^y_{n-k-1,k+1}(\Delta x, \Delta y) < \epsilon$$

for $n = 1, 2, ...K$, $k = 0, 1, ...n-1$.

*Proof:*

Since $\vec{\tilde{h}}_N(\Delta x, \Delta y)$ converges to order $K$, for any $n = 1, 2, ..., K$, and $k = 0, 1, ..., n-1$, we have

$$h^x_{n-k,k}(\Delta x, \Delta y) \to \Big[\frac{\partial^n h^x}{\partial x^{n-k} \partial y^k}(x_0, y_0)\Big] \frac{1}{(n-k)!} \frac{1}{k!} \tag{2.3a}$$

$$h^y_{n-k-1,k+1}(\Delta x, \Delta y) \to \Big[\frac{\partial^n h^y}{\partial x^{n-k-1} \partial y^{k+1}}(x_0, y_0)\Big] \frac{1}{(n-k-1)!} \frac{1}{(k+1)!} \tag{2.3b}$$

so that

$$(n-k)\, h^x_{n-k,k}(\Delta x, \Delta y) \to \Big[\frac{\partial^n h^x}{\partial x^{n-k} \partial y^k}(x_0, y_0)\Big] \frac{1}{(n-k-1)!} \frac{1}{k!} \tag{2.3c}$$

$$(k+1)\, h^y_{n-k-1,k+1}(\Delta x, \Delta y) \;\rightarrow\; \Big[\frac{\partial^n h^y}{\partial x^{n-k-1}\partial y^{k+1}}(x_0, y_0)\Big] \frac{1}{(n-k-1)!}\,\frac{1}{k!} \qquad (2.3d)$$

$$\Rightarrow \quad (n-k)\, h^x_{n-k,k}(\Delta x, \Delta y) \;+\; (k+1)\, h^y_{n-k-1,k+1}(\Delta x, \Delta y) \qquad (2.3e)$$

$$\rightarrow \Big[\frac{\partial^n h^x}{\partial x^{n-k}\partial y^k}(x_0, y_0) \;+\; \frac{\partial^n h^y}{\partial x^{n-k-1}\partial y^{k+1}}(x_0, y_0)\Big]\, \frac{1}{(n-k-1)!}\,\frac{1}{k!}.$$

But since $\vec{h}$ is a solution of the conservation law,

$$\Big[\frac{\partial^n h^x}{\partial x^{n-k}\partial y^k}(x_0, y_0) \;+\; \frac{\partial^n h^y}{\partial x^{n-k-1}\partial y^{k+1}}(x_0, y_0)\Big] \;=\; 0 \qquad (2.3f)$$

by *Theorem 2.1.* Thus,

$$(n-k)\, h^x_{n-k,k}(\Delta x, \Delta y) \;+\; (k+1)\, h^y_{n-k-1,k+1}(\Delta x, \Delta y) \;\rightarrow\; 0 \qquad (2.3g)$$

as $\Delta x \rightarrow 0$, $\Delta y \rightarrow 0$, and the theorem follows.

The meaning of *Theorem 2.3* becomes clear when we consider the divergence of $\vec{\underset{\sim}{h}}_N$. With $\vec{\underset{\sim}{h}}_N \overset{def}{=} (\underset{\sim}{h}^x_N, \underset{\sim}{h}^y_N)$ defined by (2.95) and (2.96), we have

$$\frac{\partial}{\partial x}\, \underset{\sim}{h}^x_N(x,y) \;=\; \sum_{n=1}^{N}\sum_{k=0}^{n-1} (n-k)\, h^x_{n-k,k}(x-x_0)^{n-k-1}\,(y-y_0)^k \qquad (2.99a)$$

$$\frac{\partial}{\partial y}\, \underset{\sim}{h}^y_N(x,y) \;=\; \sum_{n=1}^{N}\sum_{k=1}^{n} k\, h^y_{n-k,k}(x-x_0)^{n-k}\,(y-y_0)^{k-1}$$

$$=\; \sum_{n=1}^{N}\sum_{k=0}^{n-1} (k+1)\, h^y_{n-k-1,k+1}(x-x_0)^{n-k-1}\,(y-y_0)^k \qquad (2.99b)$$

so that

$$\vec{\nabla}\cdot\vec{\underset{\sim}{h}}_N \;=\; \frac{\partial}{\partial x}\, \underset{\sim}{h}^x_N(x,y) \;+\; \frac{\partial}{\partial y}\, \underset{\sim}{h}^y_N(x,y) \;= \qquad (2.100)$$

$$\sum_{n=1}^{N}\sum_{k=0}^{n-1} \Big[(n-k)\, h^x_{n-k,k} \;+\; (k+1)\, h^y_{n-k-1,k+1}\Big]\,(x-x_0)^{n-k-1}\,(y-y_0)^k.$$

According to *Theorem 2.3*, a necessary condition for $\vec{\underset{\sim}{h}}_N$ to converge to order $N$ is that

$$(n-k)\, h^x_{n-k,k} \;+\; (k+1)\, h^y_{n-k-1,k+1} \;\rightarrow\; 0 \qquad (2.101a)$$

as $\Delta x, \Delta y \rightarrow 0$, for $n = 1, 2, ..., N,\ k = 0, 1, ..., n-1$.

The implications of this are especially significant when it comes to numerical calculations. In general, the mechanism whereby conditions (2.101a) are satisfied depends on the

particular numerical method being used. Finite-difference methods, for example, satisfy each of the conditions (2.101a) to a certain order through the difference approximations that are used. In this case, condition (2.101a) is satisfied to a given order, say order $L$, for $n = 1$. Then for higher values of $n$, conditions (2.101a) are satisfied to an order which is less than or equal to $L$. The higher order constraints expressed by (2.101a) do not result in independent conditions for a finite-difference scheme. Rather, the higher order constraints are automatically satisfied by virtue of the difference equations employed to satisfy (2.101a) corresponding to $n = 1$.

On the other hand, when one solves for the unknown coefficients $h^x_{n-k,k}$ and $h^y_{n-k,k}$ directly, as in the present approach, each constraint associated with (2.101a) represents an independent condition. Thus, to ensure that (2.101a) is always satisfied, one should require $h^x_{n-k,k}$ and $h^y_{n-k,k}$ to satisfy

$$(n-k)\, h^x_{n-k,k} \;+\; (k+1)\, h^y_{n-k-1,k+1} \;=\; 0 \qquad (2.101b)$$

for $n = 1, 2, ..., N,\ k = 0, 1, ..., n-1$. That is, $\vec{\underset{\sim}{h}}_N$ should be a solution of the conservation law. As a result, conditions (2.101a) are not satisfied just to a certain order as in finite-difference methods, but rather are satisfied identically.

When the coefficients $h^x_{n-k,k}$ and $h^y_{n-k,k}$ are functions of intermediate variables (as in the case of the Navier-Stokes equations), each constraint associated with (2.101b) must be expressed in terms of the intermediate variables. We now show that it is possible to obtain these constraints directly without the need to re-express (2.101b) in terms of the intermediate variables.

Let $\vec{h} = (h^x, h^y)$ be defined on a domain $\mathcal{D}$ such that $h^x$ and $h^y$ are analytic at the point $(x_0, y_0)$ in $\mathcal{D}$, with series expansions that converge for all $(x, y)$ in $\mathcal{D}$. We then also have the convergent series expressed by (2.84) and (2.85). If $\vec{h}$ is a solution to (2.77), then its partial derivatives satisfy (2.79) for all $(x, y)$, and in particular for $(x_0, y_0)$. On the other hand, suppose that the partial derivatives of $h^x$ and $h^y$ satisfy (2.79) at $(x_0, y_0)$. Since $\frac{\partial h^x}{\partial x}$ and $\frac{\partial h^y}{\partial y}$ are each convergent for all $(x, y)$ in $\mathcal{D}$, so is their sum. Let RHS(2.84) and RHS(2.85) denote the right hand sides of (2.84) and (2.85), respectively. Then all the coefficients in the infinite series $\frac{\partial h^x}{\partial x} + \frac{\partial h^y}{\partial y}$ = RHS(2.84) + RHS(2.85) are zero. Hence, $\frac{\partial h^x}{\partial x} + \frac{\partial h^y}{\partial y} = 0$, so that $\vec{h}$ is a solution of (2.77). We have established the following corollary to *Theorem 2.1*.

*Corollary 2.1* Let $\vec{h} = (h^x, h^y)$ be defined on a domain $\mathcal{D}$ of $E_2$, and let $h^x$ and $h^y$ be analytic at the point $(x_0, y_0)$ in $\mathcal{D}$, with Taylor series expansions that converge for all $(x, y)$ in $\mathcal{D}$. Then, $\vec{h}$ satisfies $\vec{\nabla} \cdot \vec{h} = 0$ throughout $\mathcal{D}$ if and only if its partial derivatives satisfy condition (2.79) at the point $(x_0, y_0)$.

Since a polynomial is everywhere analytic, *Corollary 2.1* applies to the expansions (2.95) and (2.96). To ensure that $\vec{\underset{\sim}{h}}_N$ is a solution of (2.77), it is sufficient to require the

partial derivatives of $\underset{\sim}{h}^x_N$ and $\underset{\sim}{h}^y_N$ to satisfy (2.79) at the point $(x_0, y_0)$.

We now illustrate this by way of the $x$-momentum equation. In view of *Theorem 2.3*, we require the second-order expansion $\vec{\underset{\sim}{h}}_{XM}$ to be a solution of the governing conservation law. Applying *Corollary 2.1*, we first require $\vec{\underset{\sim}{h}}_{XM}$ to satisfy (2.80) at the cell center $(x_i, y_j)$ of $SE(i,j)$:

$$\frac{\partial}{\partial x}(\underset{\sim}{u}^2 + \underset{\sim}{p} - \underset{\sim}{\tau}_{xx}) + \frac{\partial}{\partial y}(\underset{\sim}{u}\,\underset{\sim}{v} - \underset{\sim}{\tau}_{xy}) =$$

$$2\,\underset{\sim}{u}\frac{\partial}{\partial x}(\underset{\sim}{u}) + \frac{\partial}{\partial x}(\underset{\sim}{p}) - \frac{\partial}{\partial x}(\underset{\sim}{\tau}_{xx}) + [\frac{\partial}{\partial y}(\underset{\sim}{u})]\underset{\sim}{v} + \underset{\sim}{u}[\frac{\partial}{\partial y}(\underset{\sim}{v})] - \frac{\partial}{\partial y}(\underset{\sim}{\tau}_{xy}) = 0. \quad (2.102)$$

We may then immediately write

$$2\,u_{0,0}\,u_{1,0} + p_{1,0} - \frac{2}{3Re_L}(4u_{2,0} - v_{1,1}) + u_{0,1}\,v_{0,0} + u_{0,0}\,v_{0,1} - \frac{1}{Re_L}(2u_{0,2} + v_{1,1}) =$$

$$u_{1,0}\,u_{0,0} + u_{0,1}\,v_{0,0} + p_{1,0} - \frac{1}{Re_L}[(2\,u_{0,2} + v_{1,1}) + \frac{2}{3}(4\,u_{2,0} - v_{1,1})] = 0 \quad (2.103)$$

where the equality follows from (2.56). The first-order constraint expressed by (2.103) is identical to the $x$-momentum flux conservation constraint (2.63).

We now require $\vec{\underset{\sim}{h}}_{XM}$ to satisfy (2.81a) and (2.81b) at $(x_i, y_j)$. Differentiating (2.102) with respect to $x$ and setting the resulting constant term to zero, we obtain the second-order constraint

$$2(2\,u_{0,0}\,u_{2,0} + u^2_{1,0} + p_{2,0}) + u_{1,1}\,v_{0,0} + v_{1,1}\,u_{0,0} + u_{1,0}\,v_{0,1} + u_{0,1}\,v_{1,0} = 0. \quad (2.104)$$

Similarly, differentiating (2.102) with respect to $y$, we obtain

$$2(u_{0,0}\,v_{0,2} + v_{0,0}\,u_{0,2} + v_{0,1}\,u_{0,1}) + 2\,u_{1,1}\,u_{0,0} + 2\,u_{1,0}\,u_{0,1} + p_{1,1} = 0. \quad (2.105)$$

In the same manner, we obtain the second-order constraints

$$2\,u_{2,0} + v_{1,1} = 0 \quad (2.106)$$

$$2\,v_{0,2} + u_{1,1} = 0 \quad (2.107)$$

$$2(u_{0,0}\,v_{2,0} + v_{0,0}\,u_{2,0} + v_{1,0}\,u_{1,0}) + 2\,v_{1,1}\,v_{0,0} + 2\,v_{1,0}\,v_{0,1} + p_{1,1} = 0 \quad (2.108)$$

$$2(2\,v_{0,0}\,v_{0,2} + v^2_{0,1} + p_{0,2}) + u_{1,1}\,v_{0,0} + v_{1,1}\,u_{0,0} + u_{1,0}\,v_{0,1} + u_{0,1}\,v_{1,0} = 0 \quad (2.109)$$

for $\vec{\underset{\sim}{h}}_M$ and $\vec{\underset{\sim}{h}}_{YM}$, respectively. The first-order constraints for $\vec{\underset{\sim}{h}}_M$ and $\vec{\underset{\sim}{h}}_{YM}$ are identical to (2.56) and (2.70).

By requiring $\vec{\underset{\sim}{h}}_M$, $\vec{\underset{\sim}{h}}_{XM}$, and $\vec{\underset{\sim}{h}}_{YM}$ to be solutions of the governing conservation law, we automatically ensure that local flux conservation is satisfied. This is a general result, which follows from the divergence theorem. Any function with zero divergence will satisfy local flux conservation. Thus, requiring the discrete flux vectors to obey the conservation law ensures the satisfaction of both local flux conservation and the necessary conditions for convergence to order $N$.

The formal order of accuracy of $\vec{\underset{\sim}{h}}_M$, $\vec{\underset{\sim}{h}}_{XM}$, and $\vec{\underset{\sim}{h}}_{YM}$ as approximations to $\vec{h}_M$, $\vec{h}_{XM}$, and $\vec{h}_{YM}$ is third-order. If third-order accuracy is maintained throughout the full development of a specific scheme, then the order of accuracy of the scheme remains third-order. An ideal error bound for the local expansions would then be given by (2.90) and (2.91).

## III. Application to the Thin Airfoil Boundary Layer Problem

We now construct a specific scheme for the thin airfoil boundary layer problem. Consider the mesh shown in Figure 3. The airfoil lies on the $x$ axis between $x = 0$ and $x = 1$, and the grid is stretched in the plus and minus $y$ directions. (The nonuniform spacing does not introduce any new complication since the discrete equations presented in the previous section still apply if $\Delta x$ and $\Delta y$ are replaced by $\Delta x_i$ and $\Delta y_j$.) Note that our mesh includes both an upstream and wake region.

Let $N_i$ and $N_j$ denote the number of solution elements in the $x$ and $y$ directions, respectively. There are six unknowns per cell for each of the three discrete variables $\underset{\sim}{u}$, $\underset{\sim}{v}$, and $\underset{\sim}{p}$. There are then $18N_iN_j$ unknowns altogether, and we require $18N_iN_j$ conditions to have a closed system of equations.

The first-order constraints (2.56), (2.63), and (2.70), together with the second-order constraints (2.104) – (2.109), immediately provide 9 $N_iN_j$ conditions. These conditions ensure that the discrete flux vectors $\vec{\underset{\sim}{h}}_M$, $\vec{\underset{\sim}{h}}_{XM}$, and $\vec{\underset{\sim}{h}}_{YM}$ are solutions of the governing conservation law (equation 2.77).

We must also require that mass and momentum fluxes balance across each vertical and horizontal interface in the mesh. This gives $3N_j(N_i - 1) + 3N_i(N_j - 1) - 3N_a$ conditions, where $N_a$ is the number of solution elements between the airfoil leading and trailing edges.

Boundary conditions account for an additional $4N_i + 3N_j + 4N_a$ conditions. For each cell adjacent to the airfoil, we require the mass flux through the wall face, and the $u$ velocity component at the midpoint of the wall face, to be zero. At the upstream boundary we specify the velocity, and at the downstream boundary we specify the pressure. Along the free-stream boundary cells, we specify zero $y$ gradient conditions for $\underset{\sim}{u}$ and $\underset{\sim}{v}$.

Finally, we may set

$$p_{1,1} = 0 \tag{3.1}$$

$$p_{2,0} = 0 \tag{3.2}$$

on physical grounds. These terms are negligibly small due to the nearly constant (zero) pressure gradient.*

The above conditions ensure the satisfaction of local and global flux conservation, boundary conditions, and all other relevant physical requirements. We are now free to impose any other physically realistic condition to close the system. The number of conditions needed is $N_i(N_j - 1) - N_a$. This is precisely the number of horizontal interfaces in the mesh (minus those that coincide with the airfoil). Consequently, there is an additional degree of freedom in specifying horizontal interface conditions. Following [3], we require $\underset{\sim}{u}$ to be continuous at the midpoint of each horizontal interface.

By virtue of (3.1) and (3.2), there are 16 unknowns on each solution element. However, using the local constraints (2.56), (2.63), (2.70), (2.106), (2.107), and (2.109), six of the unknowns may be eliminated in terms of other variables. The total number of unknowns that must be solved for is then $10N_iN_j$.

The discrete boundary value problem outlined above is presented in the Appendix. The equations presented there are a coupled system of second-order polynomial equations in the unknown coefficients $u_{0,0}$, $v_{0,0}$, $p_{0,0}$, etc.. Solution of this system may be accomplished very efficiently using Newton's method. Because the thin airfoil velocity field has a preferred direction, the Newton iteration generally converges to the physical solution without difficulty. An initial guess of uniform flow is usually sufficient to ensure convergence. For flows with more complicated physics, it may be necessary to use a different solution technique (e.g., a time-iterative approach).

The Jacobian matrix associated with equations A.9 – A.29 can be arranged to have the structure shown in Figure 4. The form is the same as the Jacobian matrix associated with the internal flow scheme.[3] Because the matrix is nearly block diagonal, direct inversion is a suitable choice for the Newton iteration. By employing a sub-block pivoting strategy,[3] the Jacobian matrix retains the same structure throughout the elimination process, and there is no matrix fill-in in the upper and lower diagonal blocks.

## IV. Numerical Results

In this section we present numerical results from calculations of the thin airfoil flow field at a Reynolds number of 100,000. To assess the accuracy of our results, we compare with the Blasius solution. However, due to leading edge, trailing edge, and wake effects, the Blasius boundary layer profile will not compare well with a Navier-Stokes solution over the full length of the airfoil. On the other hand, at high Reynolds numbers, the Blasius solution does provide the correct boundary layer profile over a substantial part of

*For many flows it will not be physically correct to impose conditions (3.1) and (3.2). The author is currently investigating ways of retaining both $p_{1,1}$ and $p_{2,0}$ for the more general case.

the airfoil. In particular, the Blasius solution may be used for comparison in the interior region where the leading and trailing edges are many boundary layer thicknesses away.

Information from the Blasius solution may also be used in the construction of a mesh for numerical computations. If we let $Re$ denote the Reynolds number based on the airfoil chord $c$, then the similarity relation[7,8]

$$\eta = y\sqrt{\frac{U}{2\nu x}} \tag{4.1}$$

becomes

$$\eta = \sqrt{Re}\,\frac{y}{c}\sqrt{\frac{U/U_\infty}{2(\nu/\nu_\infty)(x/c)}} \tag{4.2}$$

where all quantities except $\eta$ and $Re$ are dimensional. We may identify the free-stream velocity $U$ with $U_\infty$, and take $\frac{\nu}{\nu_\infty} = 1$ (since we assume constant viscocity). Equation 4.2 then becomes

$$\eta = \sqrt{Re}\,\frac{y}{c}\sqrt{\frac{c}{2x}}. \tag{4.3}$$

Corresponding to any $\eta$, $x$ and $y$ are related through the equation

$$\frac{y}{c} = \eta\sqrt{\frac{2}{Re}}\sqrt{\frac{x}{c}}. \tag{4.4}$$

Equation (4.4) allows us to estimate the location of the edge of the boundary layer for any fixed $\frac{x}{c}$. We take $\eta = 6.0$, corresponding to $\frac{u}{U_\infty} = 0.999999$,[8] to be the edge of the boundary layer. An estimate of the boundary layer thickness $\delta_x$ at any $\frac{x}{c}$ is then given by

$$\delta_x = 6.0\sqrt{\frac{2}{Re}}\sqrt{\frac{x}{c}}. \tag{4.5}$$

At the trailing edge we have the estimate

$$\delta_{t.e.} = 6.0\sqrt{\frac{2}{Re}}. \tag{4.6}$$

For $Re = 100{,}000$, one gets $\delta_{t.e.} = 0.0268$.

In the construction of a mesh for numerical computations, one would expect that the free-stream mesh boundaries should extend to at least a distance of $\delta_{t.e.}$ from the airfoil in order to obtain accurate results. In the present study, detailed numerical calculations were carried out with mesh boundaries located at $\pm y = \delta_{t.e.}$, $1.5\,\delta_{t.e.}$, and $2.0\,\delta_{t.e.}$, where $\delta_{t.e.} = 0.027$. For each case, calculations were performed on a grid with uniform $x$ spacing ($\Delta x = .02$) and nonuniform $y$ spacing with exponential stretching. The $y$ spacing at the wall ($\Delta y_w$) was determined on the basis of the boundary layer thickness near the leading edge of the airfoil. With $\Delta x = .02$, we should require the mesh spacing to be fine enough

to resolve the boundary layer at $x = .01$ (since we require the $u$ velocity to be continuous at the midpoint of horizontal cell interfaces). The boundary layer thickness at $x = .01$ is approximately 0.00268 (based on equation 4.5). Because the present discretization represents the $u$ velocity by a quadratic polynomial, one would expect to be able to resolve the nearly linear boundary layer profile in the near wall region with only one or two cells. Using two cells, one obtains the estimate $\Delta y_w = .00134$. However, convergence problems were encountered by the Newton's method for this value of $\Delta y_w$ (with uniform flow conditions as the starting solution). We used the slightly larger value of $\Delta y_w = .0015$ instead.

Once the wall spacing and mesh boundaries are fixed, grid stretching can be used to reduce the number of cells required to reach the outer boundary. Since we compute the flow field on both sides of the airfoil, the number of cells available to resolve the boundary layer is half the total number of cells in the $y$ direction. A systematic series of calculations performed with mesh boundaries located at $\pm y = \delta_{t.e.}$, $1.5\,\delta_{t.e.}$, and $2.0\,\delta_{t.e.}$ showed that no accuracy was gained by extending the mesh boundaries farther than $\pm y = \delta_{t.e.}$ from the airfoil. Consequently, the present discussion will deal only with results obtained from the smaller mesh.

The first series of calculations were performed on grids with uniform $x$ spacing of $\Delta x = .02$. The upstream boundary was located at $x = -.12$, and the downstream boundary at $x = 1.5$. The spacing was varied exponentially in the $y$ direction, using as few as 16 cells with exponential stretching of 22.4%, and as many as 28 cells with exponential stretching of 3.8%. In general, the agreement with the Blasius solution improved as the mesh was refined. In Figure 5 we show two of the grids that were used.

Figures 6 – 8 present comparisons of the discrete velocity $\underset{\sim}{u}$ with the Blasius solution at various $x$ locations along the airfoil. The numerical results in these figures were obtained from the grids shown in Figure 5. Note that at each $x_i$ (the $x$ nodal points), $\underset{\sim}{u}(i,j) = [u_{0,0} + u_{0,1}(y - y_j) + u_{0,2}(y - y_j)^2]_{i,j}$ is a piecewise continuous function from the wall to the free stream (See equation A.18).

Figure 6 compares $\underset{\sim}{u}$ with the Blasius solution at the airfoil leading edge ($x = .01$). The discrete velocity clearly shows the effect of the strong leading edge singularity. The Blasius similarity solution, on the other hand, does not account for the singular behavior of the flow field in this region. It is apparent from these results that two cells are sufficient to resolve the leading edge boundary layer profile.

In Figures 7 and 8 we compare with the Blasius solution at four different locations along the airfoil. The agreement steadily improves as $x$ increases. This trend continues up to about $x = .85$, where trailing edge and wake effects become significant. This can be seen from the results shown in Figure 9 a., where we plot the maximum deviation of $\underset{\sim}{u}$ from the Blasius solution as a function of $x$.

In Figure 9 b., we show the improved accuracy that is obtained by refining the mesh spacing in the $y$ direction. The exponential $y$ stretching for the five grids used in the figure was 12.5%, 9.5%, 7.1%, 5.3%, and 3.8%, respectively. The maximum deviation of $\underset{\sim}{u}$ from the Blasius solution is less than $5 \times 10^{-3}$ over a significant portion of the airfoil for all of

the grids except the coarsest one.

In Figures 6 – 8 we compared $\underset{\sim}{u}$ with the Blasius solution at fixed nodal points $x_i$. This enabled us to present a streamwise velocity profile which is continuous across cell interfaces. However, it only required using the three discrete Taylor coefficients $u_{0,0}, u_{0,1}$, and $u_{0,2}$. In Figures 10 a. and b., we compare $\underset{\sim}{u}(x_i + \frac{\Delta x_i}{2}, y_j - \frac{\Delta y_j}{2})$ with the Blasius solution (i. e., we compare at the lower right hand corner of each solution element). This comparison requires the use of all the discrete Taylor coefficients associated with $\underset{\sim}{u}$. The mesh sizes associated with Figures 10 a. and b. are indicated below the figures. The 81 x 22 grid is the same as the one used in Figure 9 b. ($\Delta x = .02$, $\Delta y_w = .0015$ with 9.5% exponential $y$ stretching). The 110 x 28 grid is refined in both the $x$ and $y$ directions ($\Delta x_{t.e.} = .007$, 2.5% exponential $x$ stretching away from the trailing edge, $\Delta y_w = .0015$, with 3.8% exponential $y$ stretching). The grids are intended to be "coarse" and "fine", respectively.

The accuracy demonstrated in Figures 10 a. and b. is comparable to that shown in Figures 7 and 8. This suggests that $\underset{\sim}{u}$ uniformly approximates the exact solution $u$ over the entire solution element. Further evidence for this is provided by the results shown in Figures 10 c. – f. In Figures 10 c. and d., comparison is made with the Blasius solution at the cell center (i. e., $u_{0,0}$ is compared with the Blasius solution). Figures 10 e. and f. show the "error" (i. e., the deviation from the Blasius solution) of the numerical results in Figures 10 a. – d.

The above results confirm that $\underset{\sim}{u}$ does indeed uniformly approximate the exact solution $u$ throughout the solution element. This is a direct consequence of requiring the discrete flux vectors to identically satisfy the governing conservation law. Since the conservation law is satisfied identically, and not just at a point, there is no preferred location within a solution element. Thus, the accuracy of the discrete approximation is essentially uniform.

One final set of results is presented in Figure 10 g. Here we compare the value of $\underset{\sim}{u}$ from adjacent solution elements at a common point on their interface. The maximum difference in the value of $\underset{\sim}{u}$ corresponding to the $i = I$ and $i = I + 1$ locations is less than 2.24 x $10^{-3}$. These results correspond to the "coarse" grid. For the "fine" grid, a similar calculation showed a maximum difference which is less than 7.7 x $10^{-4}$. Thus, $\underset{\sim}{u}$ is nearly continuous across cell interfaces.

We conclude our discussion with a presentation of numerical results from the trailing edge region. Our motivation was to determine how fine a mesh spacing is required to accurately resolve the trailing edge pressure singularity. The grids used for this purpose are shown in Figure 11. The $y$ spacing was the same for all five grids. Each grid has $\Delta y_w = .0015$, 9.5% exponential $y$ stretching, and free-stream mesh boundaries located at $\pm y = .027$. The mesh in Figure 11 a. has uniform $x$ spacing, while the other four grids are refined in the trailing edge region with exponential stretching. The value of $\Delta x$ at the trailing edge was .02, .01, .009, .008, and .007, respectively. This is denoted below each figure by "dxte = .02", etc. The exponential stretching away from the trailing edge was the same in the wake as on the airfoil. The downstream boundary was located at

approximately $x = 1.5$ for all cases.

In Figures 12 and 13 we present the numerical results. Figure 12 shows the pressure coefficient as a function of $x$. The results correspond in order to the five grids shown in Figure 11. It is remarkable how little mesh refinement is required to resolve the pressure singularity. Our results indicate a minimum value of $-.014$ for the pressure coefficient. This agrees well with the recent calculations of Srinivasan and Rubin.[9]

Figure 13 shows the streamwise velocity profile at four different $x$ locations in the trailing edge region. The results correspond to the last solution element on the airfoil and the first three solution elements in the wake.

All of the calculations associated with the present work were performed on the Cray YMP at the NASA Lewis Research Center. The CPU times ranged from 30.3 seconds for the coarsest grid (81 x 16) to 170 seconds for the finest grid (110 x 28). Most of the calculations took about 80 CPU seconds. Each case was started from uniform flow and converged in nine or ten Newton iterations to a maximum residual error which was less than $10^{-10}$.

The above CPU times can be considerably reduced by using a previous solution, rather than uniform flow, as the initial guess for Newton's method. Further reductions can be achieved by using equations A.9 – A.11 to eliminate additional variables from the discrete system of equations that must be solved. If three more variables are eliminated, the block sizes associated with the Jacobian matrix can be reduced from $10N_j$ to $7N_j$. Since the operation count for Gaussian elimination is $O(n^3)$, where $n$ is the block size, the CPU times could be reduced by a factor of $(\frac{10}{7})^3 \approx 2.9$. Combined with using an improved initial guess, we estimate that the CPU times can be reduced by a factor of about five without making any changes to the matrix solution technique.

## Summary

In this paper we have presented a new numerical scheme for the solution of the thin airfoil boundary layer problem. The results presented above have shown (i) the ability of the scheme to accurately resolve the thin airfoil flow field on grids which are much coarser than those used by conventional numerical methods, (ii) the uniform accuracy of the discrete solution throughout the solution element, and (iii) a nearly continuous discrete solution across cell interfaces.

In Section II, using both an integral and differential approach, we rederived the discrete flux conservation equations presented in [3]. Here we presented a simpler method for deriving the flux expressions at cell interfaces, and provided a systematic and rigorous derivation of the conditions used to simulate the differential form of the conservation laws. A generalized concept of convergence was introduced, and necessary conditions for the order-$N$ convergence of a discrete approximation were derived. In addition, necessary and sufficient conditions for a discrete approximation to satisfy a conservation law in $E_2$ were presented. An ideal error bound on the discrete solution was also derived.

We conclude with the following remarks. First, the theoretical results established in Section II C. are applicable to any conservation law in $E_2$, and their analogues in higher dimensions readily follow. Second, extension of the present scheme to three dimensions is straightforward and follows naturally from the 2-D formulation. Third, higher-order schemes for the Navier-Stokes equations may be very efficiently constructed using the methodology and theory presented in Section II. Fourth, a faithful simulation of the conservation laws associated with the Navier-Stokes equations requires the rigorous enforcement of both local and global flux conservation. This is accomplished most naturally through an integral formulation. At the same time, the integral and differential forms of the conservation laws cannot be divorced from each other. Thus, a fundamental tenet of the space-time solution element method is the rigorous enforcement of both the integral and differential forms of the governing conservation laws. Finally, the results presented in Section IV have clearly demonstrated the convergence of the discrete solution as the mesh spacing is refined. The uniform accuracy over the solution element suggests that the convergence is of order two. An analysis of the order of convergence will be provided in a forthcoming paper.

## References


[1] Chang, S.C. and To, W.M., "A New Numerical Framework for Solving Conservation Laws – The Method of Space-Time Conservation Element and Solution Element," NASA TM 104495, August, 1991.

[2] Chang, S.C. and To, W.M., "A Brief Description of a New Numerical Framework for Solving Conservation Laws – The Method of Space-Time Conservation Element and Solution Element," *Proceedings of the Thirteenth International Conference on Numerical Methods in Fluid Dynamics*, Rome, Italy, 1992, Napolitano, M. and Sabetta, F., eds., Lecture Notes in Physics 414, Springer-Verlag. Also published as NASA TM 105757.

[3] Scott, J.R. and Chang, S.C., "A New Flux Conserving Newton's Method Scheme for the Two-Dimensional, Steady Navier-Stokes Equations," NASA TM 106160, June, 1993.

[4] Chang, S.C., "New Developments in the the Method of Space-Time Conservation Element and Solution Element – Application to the Euler and Navier-Stokes Equations," NASA TM 106226, August, 1993.

[5] Anderson, D.A., Tannehill, J.C., and Pletcher, R.H., *Computational Fluid Mechanics and Heat Transfer*, (Hemisphere, 1984), pp. 190-193.

[6] Buck, R.C., *Advanced Calculus*, 3rd. ed., International Series in Pure and Applied Mathematics, Spanier, E.H., Springer, G., and Davis, P.J., Consulting Eds., (McGraw-Hill, 1978), p. 152.

[7] Schlichting, H., *Boundary-Layer Theory*, 7th. ed., McGraw-Hill Series in Mechanical Engineering, Holman, J.P., Consulting Ed., (McGraw-Hill, 1979), pp. 135-140.

[8] White, F.M., *Viscous Fluid Flow*, (McGraw-Hill, 1974), pp. 261-266.

[9] Srinivasan, K. and Rubin, S.G., "Segmented Multigrid Domain Decomposition Procedure For Incompressible Viscous Flows", *International Journal For Numerical Methods in Fluids*, Vol. 15, pp. 1333-1355, 1992.

## Appendix

$$p_{1,1} = 0 \tag{A.1}$$

$$p_{2,0} = 0 \tag{A.2}$$

$$v_{0,1} = -u_{1,0} \tag{A.3}$$

$$v_{1,1} = -2u_{2,0} \tag{A.4}$$

$$u_{1,1} = -2v_{0,2} \tag{A.5}$$

$$p_{1,0} = -(u_{1,0}u_{0,0} + u_{0,1}v_{0,0}) + \frac{2}{Re_L}(u_{2,0} + u_{0,2}) \tag{A.6}$$

$$p_{0,1} = -(v_{1,0}u_{0,0} - u_{1,0}v_{0,0}) + \frac{2}{Re_L}(v_{2,0} + v_{0,2}) \tag{A.7}$$

$$p_{0,2} = (u_{0,0}u_{2,0} - v_{0,0}v_{0,2}) - \frac{1}{2}(u_{1,0}^2 + u_{0,1}v_{1,0}) \tag{A.8}$$

Second-Order Constraints:

$$\left[2(u_{0,0}u_{2,0} - v_{0,0}v_{0,2}) + u_{1,0}^2 + u_{0,1}v_{1,0}\right]_{i,j} = 0 \tag{A.9}$$

$$\left[v_{0,0}u_{0,2} - u_{0,0}v_{0,2}\right]_{i,j} = 0 \tag{A.10}$$

$$\left[u_{0,0}v_{2,0} - v_{0,0}u_{2,0}\right]_{i,j} = 0 \tag{A.11}$$

Balance of Mass and Momementum Fluxes Across Vertical Interfaces:

$$\left[\frac{\Delta y^2}{12}u_{0,2} + \frac{\Delta x^2}{4}u_{2,0} + \frac{\Delta x}{2}u_{1,0} + u_{0,0}\right]_{i,j} \tag{A.12}$$

$$-\left[\frac{\Delta y^2}{12}u_{0,2} + \frac{\Delta x^2}{4}u_{2,0} - \frac{\Delta x}{2}u_{1,0} + u_{0,0}\right]_{i+1,j} = 0$$

$$\left[\frac{\Delta y^2}{12}(2\,u_{0,2}\,u_{0,0} + u_{0,1}^2 + u_{2,0}\,u_{0,0} - v_{0,2}\,v_{0,0} - \frac{u_{1,0}^2}{2} - \frac{u_{0,1}v_{1,0}}{2}) + \frac{\Delta x^2}{4}(2\,u_{2,0}\,u_{0,0} + u_{1,0}^2)\right.$$

$$\left. - \frac{\Delta x}{2}[v_{0,0}\,u_{0,1} - u_{0,0}\,u_{1,0} - \frac{2}{Re_L}(u_{0,2} - u_{2,0})] + p_{0,0} - \frac{2}{Re_L}u_{1,0} + u_{0,0}^2\right]_{i,j}$$

$$- \left[\frac{\Delta y^2}{12}(2\,u_{0,2}\,u_{0,0} + u_{0,1}^2 + u_{2,0}\,u_{0,0} - v_{0,2}\,v_{0,0} - \frac{u_{1,0}^2}{2} - \frac{u_{0,1}v_{1,0}}{2}) + \frac{\Delta x^2}{4}(2\,u_{2,0}\,u_{0,0} + u_{1,0}^2)\right.$$

$$\left. + \frac{\Delta x}{2}[v_{0,0}\,u_{0,1} - u_{0,0}\,u_{1,0} - \frac{2}{Re_L}(u_{0,2} - u_{2,0})] + p_{0,0} - \frac{2}{Re_L}u_{1,0} + u_{0,0}^2\right]_{i+1,j}$$

$$= 0 \qquad \text{(A.13)}$$

$$\left[\frac{\Delta y^2}{12}(v_{0,2}\,u_{0,0} + u_{0,2}\,v_{0,0} - u_{1,0}\,u_{0,1}) + \frac{\Delta x^2}{4}(v_{2,0}\,u_{0,0} + u_{2,0}\,v_{0,0} + v_{1,0}\,u_{1,0})\right.$$

$$\left. + \frac{\Delta x}{2}[u_{0,0}\,v_{1,0} + v_{0,0}\,u_{1,0} - \frac{2}{Re_L}(v_{2,0} - v_{0,2})] - \frac{1}{Re_L}(u_{0,1} + v_{1,0}) + v_{0,0}\,u_{0,0}\right]_{i,j}$$

$$- \left[\frac{\Delta y^2}{12}(v_{0,2}\,u_{0,0} + u_{0,2}\,v_{0,0} - u_{1,0}\,u_{0,1}) + \frac{\Delta x^2}{4}(v_{2,0}\,u_{0,0} + u_{2,0}\,v_{0,0} + v_{1,0}\,u_{1,0})\right.$$

$$\left. - \frac{\Delta x}{2}[u_{0,0}\,v_{1,0} + v_{0,0}\,u_{1,0} - \frac{2}{Re_L}(v_{2,0} - v_{0,2})] - \frac{1}{Re_L}(u_{0,1} + v_{1,0}) + v_{0,0}\,u_{0,0}\right]_{i+1,j}$$

$$= 0 \qquad \text{(A.14)}$$

Balance of Mass and Momementum Fluxes Across Horizontal Interfaces:

$$\left[\frac{\Delta x^2}{12}v_{2,0} + \frac{\Delta y^2}{4}v_{0,2} - \frac{\Delta y}{2}u_{1,0} + v_{0,0}\right]_{i,j} \qquad \text{(A.15)}$$

$$- \left[\frac{\Delta x^2}{12}v_{2,0} + \frac{\Delta y^2}{4}v_{0,2} + \frac{\Delta y}{2}u_{1,0} + v_{0,0}\right]_{i,j+1} = 0$$

$$\left[\frac{\Delta x^2}{12}(u_{2,0}\,v_{0,0} + v_{2,0}\,u_{0,0} + u_{1,0}\,v_{1,0}) + \frac{\Delta y^2}{4}(u_{0,2}\,v_{0,0} + v_{0,2}\,u_{0,0} - u_{0,1}\,u_{1,0})\right.$$

$$\left. + \frac{\Delta y}{2}\left[v_{0,0}\,u_{0,1} - u_{0,0}\,u_{1,0} - \frac{2}{Re_L}(u_{0,2} - u_{2,0})\right] - \frac{1}{Re_L}(u_{0,1} + v_{1,0}) + u_{0,0}\,v_{0,0}\right]_{i,j}$$

$$- \left[\frac{\Delta x^2}{12}(u_{2,0}\,v_{0,0} + v_{2,0}\,u_{0,0} + u_{1,0}\,v_{1,0}) + \frac{\Delta y^2}{4}(u_{0,2}\,v_{0,0} + v_{0,2}\,u_{0,0} - u_{0,1}\,u_{1,0})\right.$$

$$\left. - \frac{\Delta y}{2}\left[v_{0,0}\,u_{0,1} - u_{0,0}\,u_{1,0} - \frac{2}{Re_L}(u_{0,2} - u_{2,0})\right] - \frac{1}{Re_L}(u_{0,1} + v_{1,0}) + u_{0,0}\,v_{0,0}\right]_{i,j+1}$$

$$= 0 \qquad \text{(A.16)}$$

$$\left[\frac{\Delta x^2}{12}(2\,v_{2,0}\,v_{0,0} + v_{1,0}^2) + \frac{\Delta y^2}{4}(v_{0,2}\,v_{0,0} + u_{2,0}\,u_{0,0} + \frac{1}{2}u_{1,0}^2 - \frac{1}{2}u_{0,1}v_{1,0})\right.$$

$$\left. - \frac{\Delta y}{2}[u_{0,0}\,v_{1,0} + v_{0,0}\,u_{1,0} - \frac{2}{Re_L}(v_{2,0} - v_{0,2})] + p_{0,0} + \frac{2}{Re_L}u_{1,0} + v_{0,0}^2\right]_{i,j}$$

$$- \left[\frac{\Delta x^2}{12}(2\,v_{2,0}\,v_{0,0} + v_{1,0}^2) + \frac{\Delta y^2}{4}(v_{0,2}\,v_{0,0} + u_{2,0}\,u_{0,0} + \frac{1}{2}u_{1,0}^2 - \frac{1}{2}u_{0,1}v_{1,0})\right.$$

$$\left. + \frac{\Delta y}{2}[u_{0,0}\,v_{1,0} + v_{0,0}\,u_{1,0} - \frac{2}{Re_L}(v_{2,0} - v_{0,2})] + p_{0,0} + \frac{2}{Re_L}u_{1,0} + v_{0,0}^2\right]_{i,j+1}$$

$$= 0 \qquad \text{(A.17)}$$

Continuity of $\underline{u}$ Across Horizontal Interfaces:

$$\left[\frac{\Delta y^2}{4}u_{0,2} + \frac{\Delta y}{2}u_{0,1} + u_{0,0}\right]_{i,j} - \left[\frac{\Delta y^2}{4}u_{0,2} - \frac{\Delta y}{2}u_{0,1} + u_{0,0}\right]_{i,j+1} = 0 \qquad \text{(A.18)}$$

Airfoil Boundary Conditions:

Lower Surface

$$\left[\frac{\Delta y^2}{4}\,u_{0,2} + \frac{\Delta y}{2}\,u_{0,1} + u_{0,0}\right]_i = 0 \tag{A.19}$$

$$\left[\frac{\Delta x^2}{12}\,v_{2,0} + \frac{\Delta y^2}{4}\,v_{0,2} - \frac{\Delta y}{2}\,u_{1,0} + v_{0,0}\right]_i = 0 \tag{A.20}$$

Upper Surface

$$\left[\frac{\Delta y^2}{4}\,u_{0,2} - \frac{\Delta y}{2}\,u_{0,1} + u_{0,0}\right]_i = 0 \tag{A.21}$$

$$\left[\frac{\Delta x^2}{12}\,v_{2,0} + \frac{\Delta y^2}{4}\,v_{0,2} + \frac{\Delta y}{2}\,u_{1,0} + v_{0,0}\right]_i = 0 \tag{A.22}$$

Upstream Boundary Conditions:

$$\left[\frac{\Delta x^2}{4}\,u_{2,0} - \frac{\Delta x}{2}\,u_{1,0} + u_{0,0}\right]_j - u_\infty = 0 \tag{A.23}$$

$$\left[\frac{\Delta x^2}{4}\,v_{2,0} - \frac{\Delta x}{2}\,v_{1,0} + v_{0,0}\right]_j = 0 \tag{A.24}$$

Downstream Boundary Condition:

$$\left[p_{0,0}\right]_j - p_e = 0 \tag{A.25}$$

Free-Stream Boundary Conditions:

Lower Boundary

$$\left[-\Delta y\,u_{0,2} + u_{0,1}\right]_i = 0 \tag{A.26}$$

$$\left[-\Delta y\,v_{0,2} - u_{1,0}\right]_i = 0 \tag{A.27}$$

Upper Boundary

$$\left[\Delta y\,u_{0,2} + u_{0,1}\right]_i = 0 \tag{A.28}$$

$$\left[\Delta y\,v_{0,2} - u_{1,0}\right]_i = 0 \tag{A.29}$$

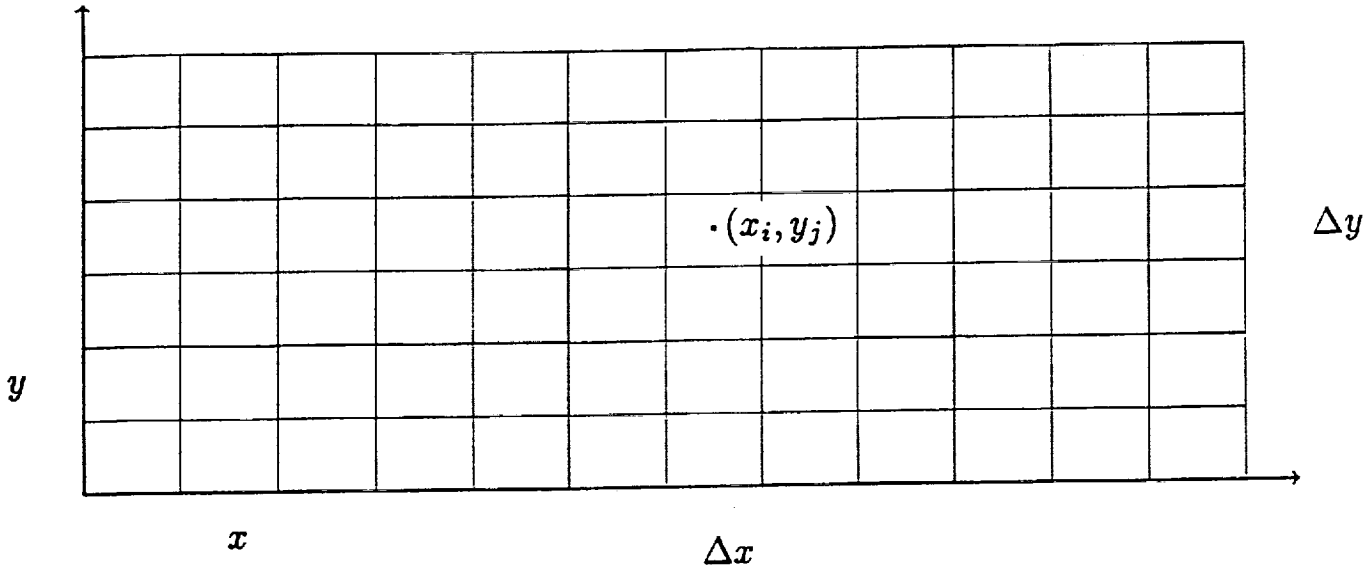


**Figure 1. Discretization of $E_2$.**

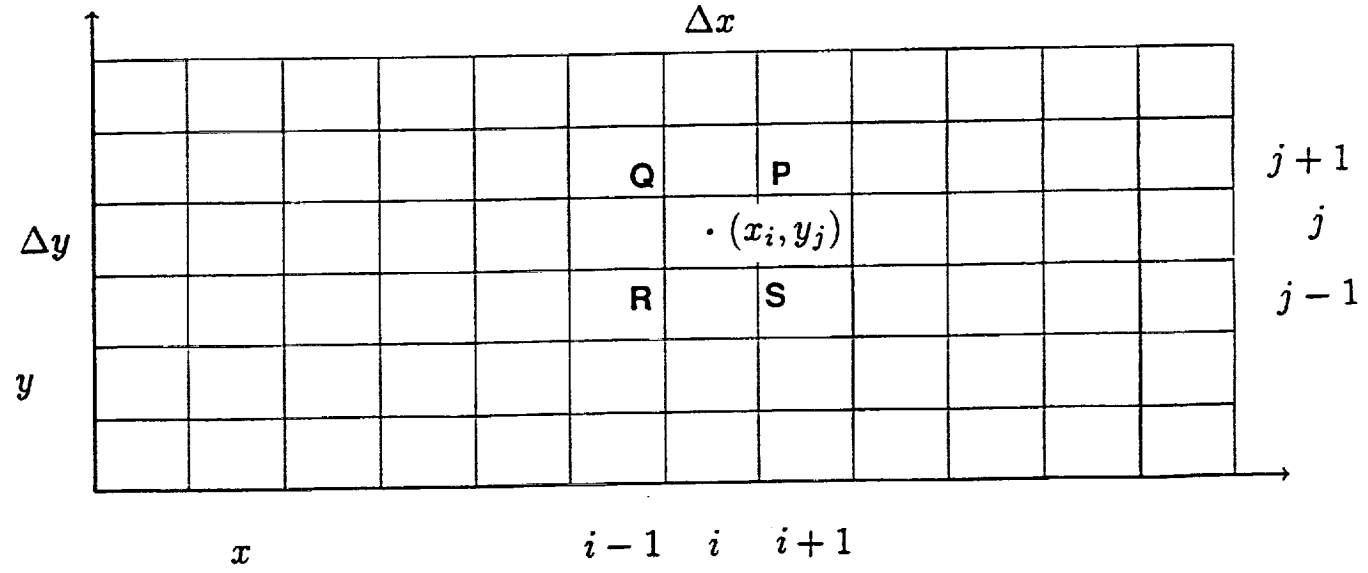


**Figure 2. Orientation for Line Integration Around S(CE(i,j)).**

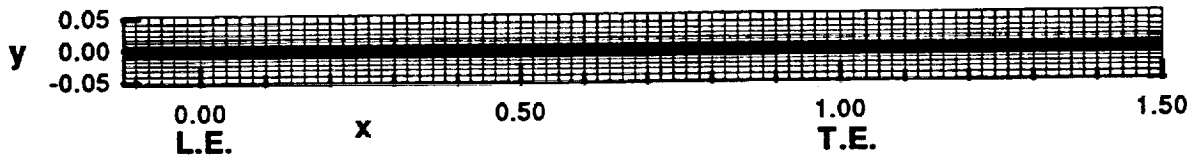


**Figure 3. Computational grid for a thin (flat-plate) airfoil.**

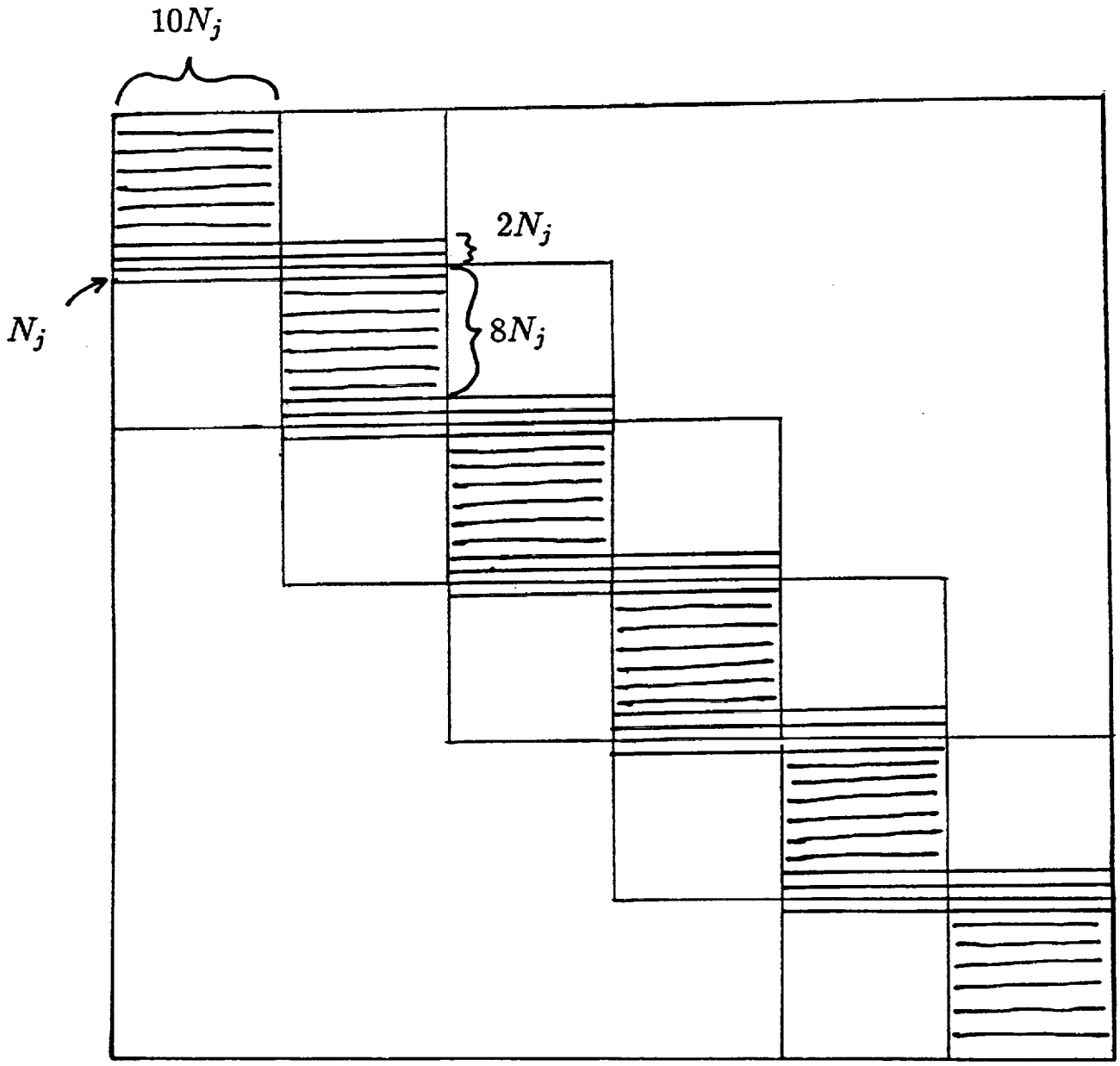


**Figure 4. Jacobian Matrix Structure.**

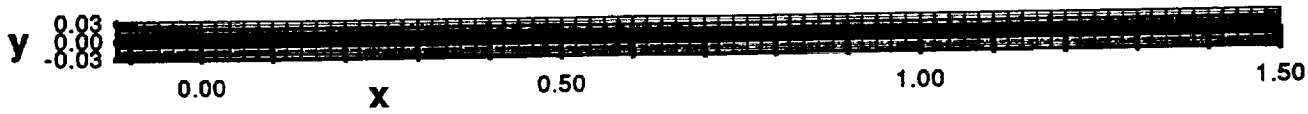


Figure 5 a. 81 x 20 computational grid with 12.5% exponential y stretching.


Figure 5 b. 81 x 28 computational grid with 3.8% exponential y stretching.

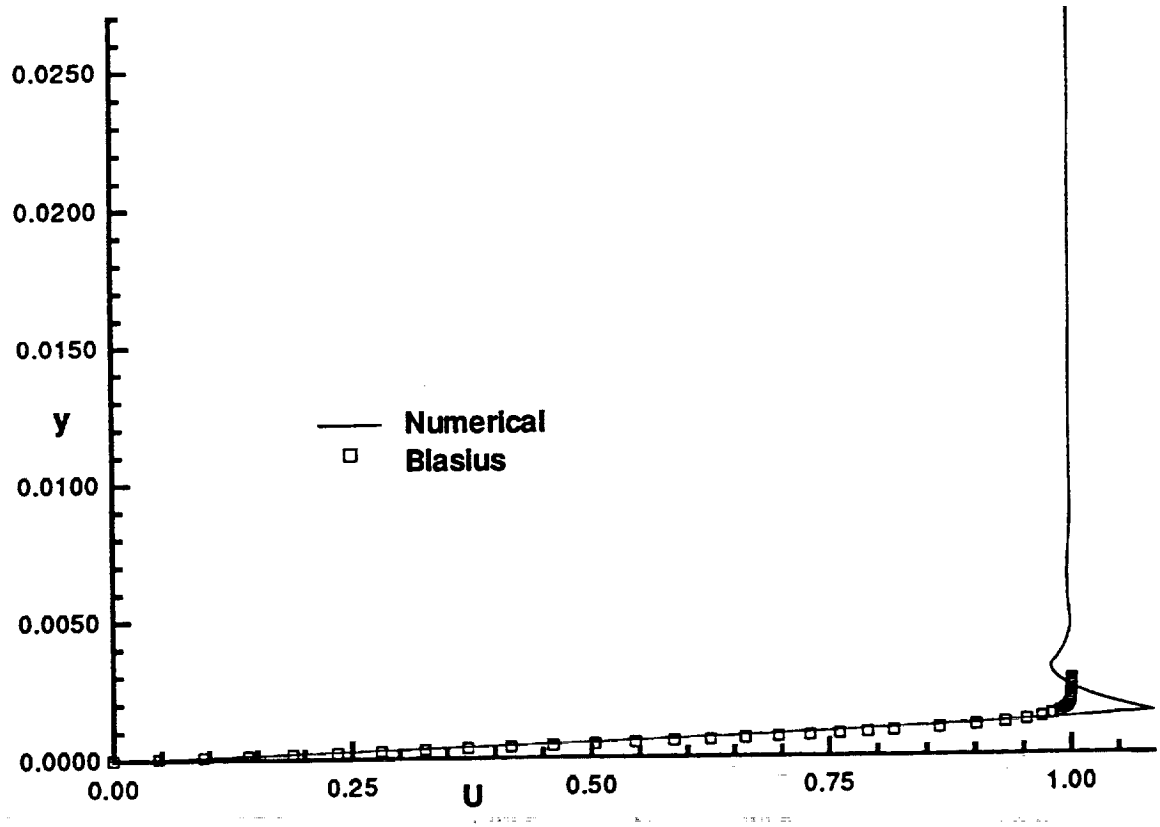


Figure 6. Comparison of numerical results and Blasius solution at airfoil leading edge (x = .01). Calculations performed on an 81 x 20 grid with 12.5% exponential y stretching.

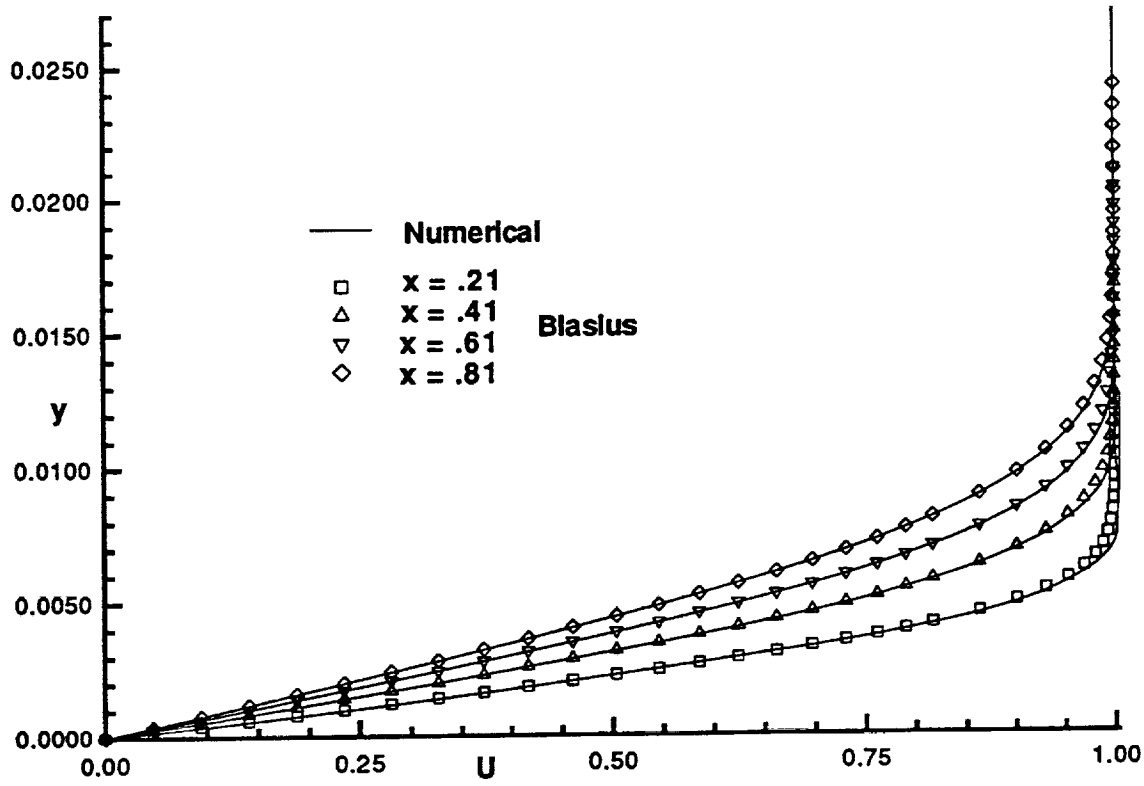


**Figure 7. Comparison of numerical results and Blasius solution at x = .21, .41, .61, and .81. Calculations performed on an 81 x 20 grid with 12.5% exponential y stretching.**

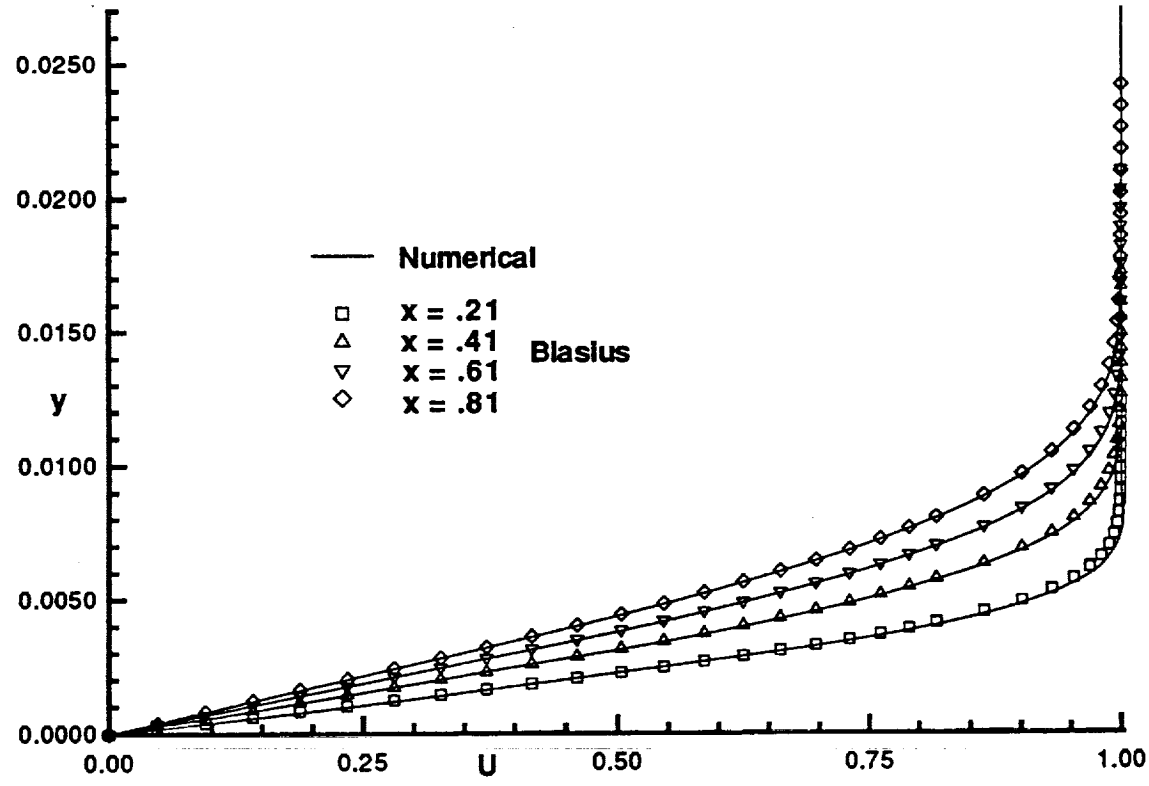


**Figure 8. Comparison of numerical results and Blasius solution at x = .21, .41, .61, and .81. Calculations performed on an 81 x 28 grid with 3.8% exponential y stretching.**

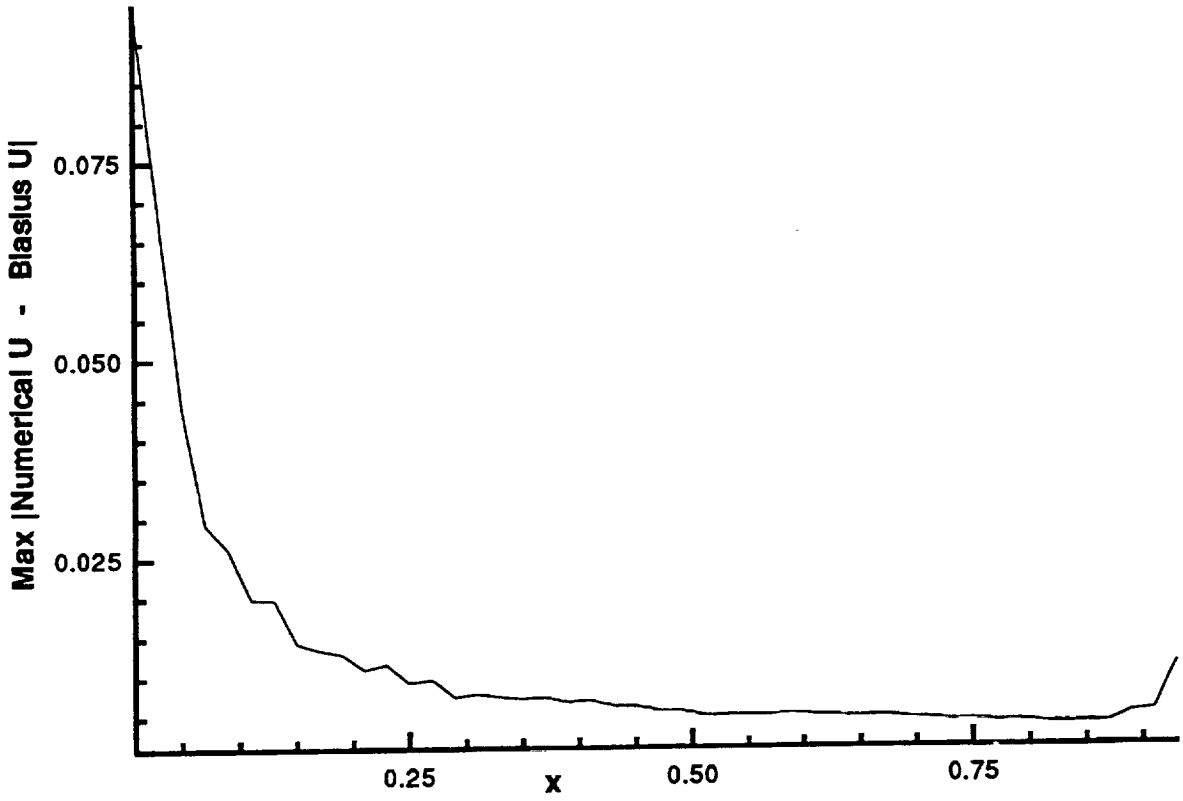


Figure 9 a. Maximum deviation of predicted streamwise velocity from Blasius solution as a function of x. 81 x 20 grid with 12.5% exponential y stretching.

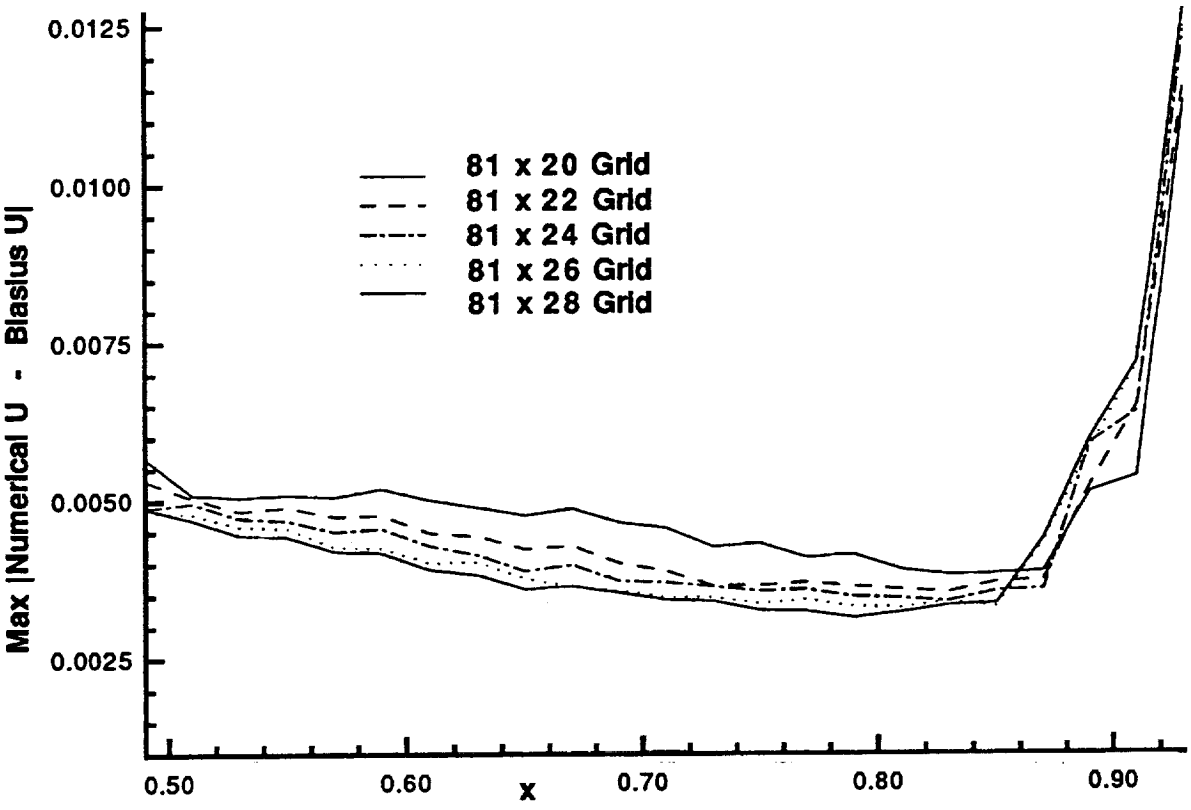


Figure 9 b. Effect of mesh refinement on deviation from Blasius solution.

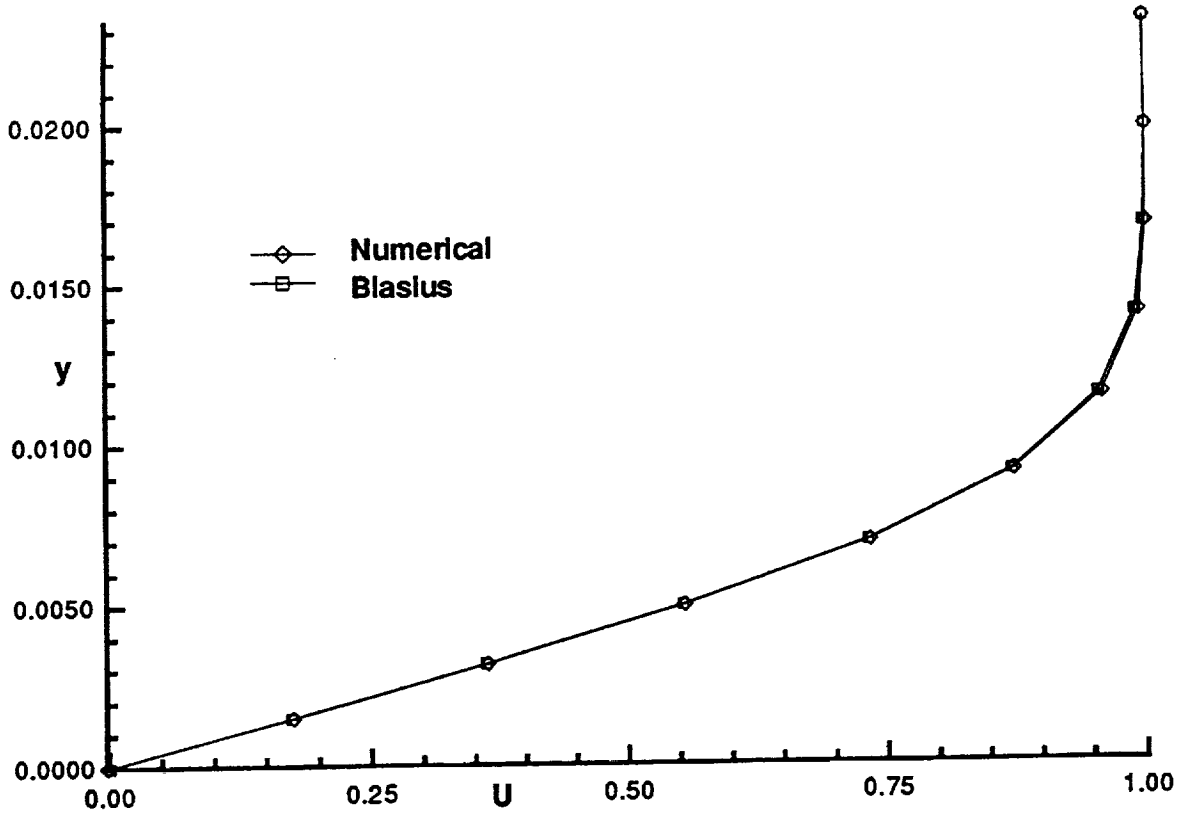


Figure 10 a. Comparison of numerical results and Blasius solution at x = .82. Comparison is at the lower right hand corner of each solution element. 81 x 22 grid.

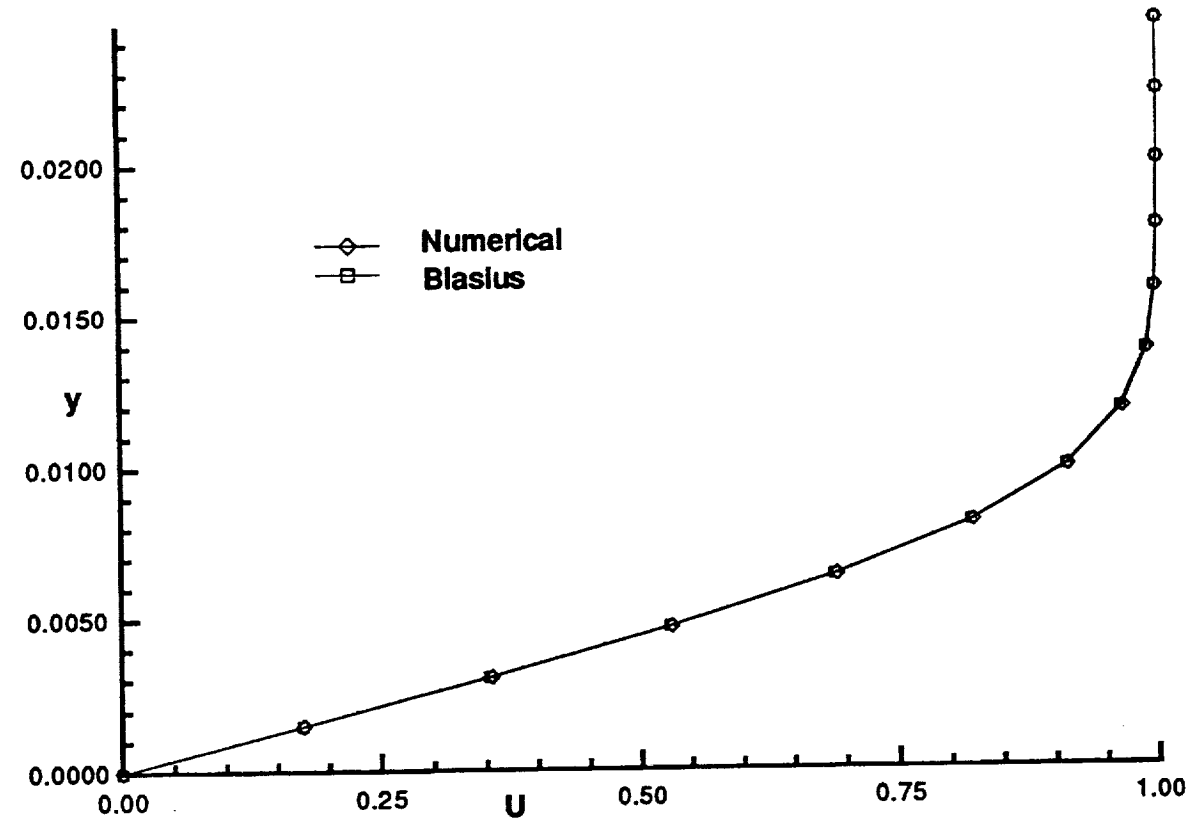


Figure 10 b. Comparison of numerical results and Blasius solution at x = .822. Comparison is at the lower right hand corner of each solution element. 110 x 28 grid.

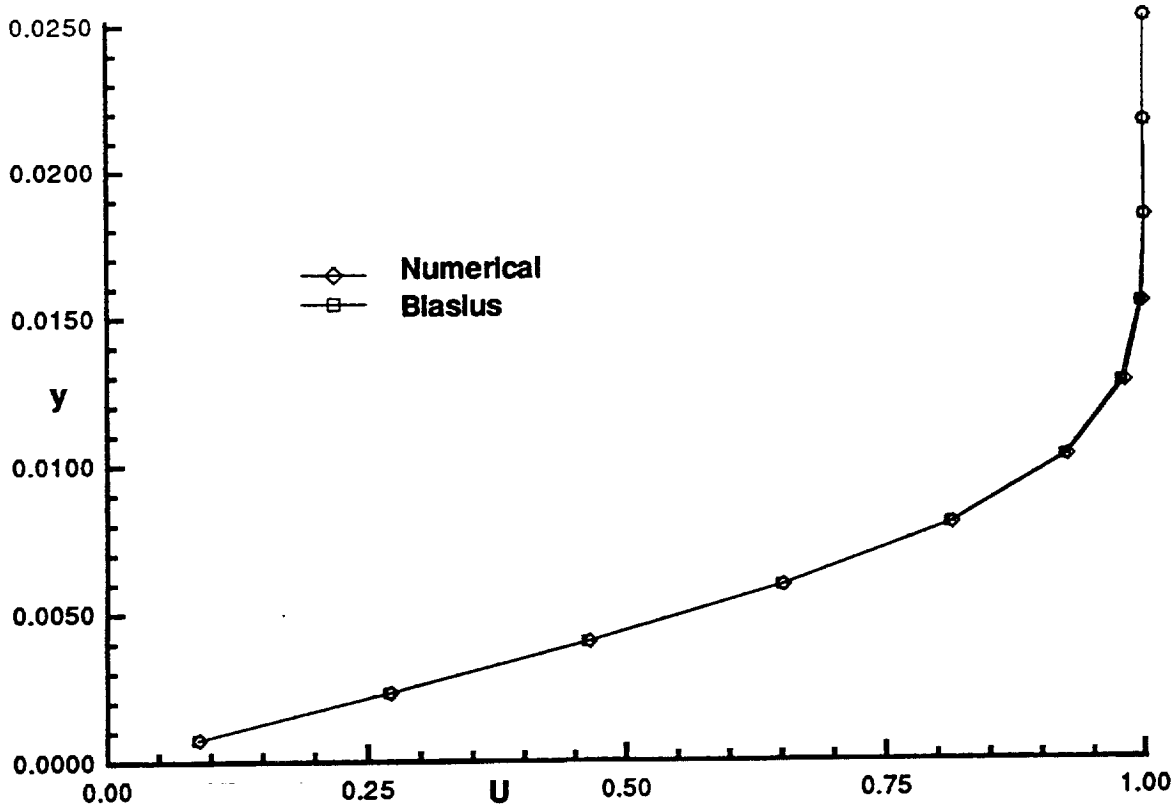


**Figure 10 c. Comparison of numerical results and Blasius solution at x = .81. Comparison is at the cell center of each solution element. 81 x 22 grid.**

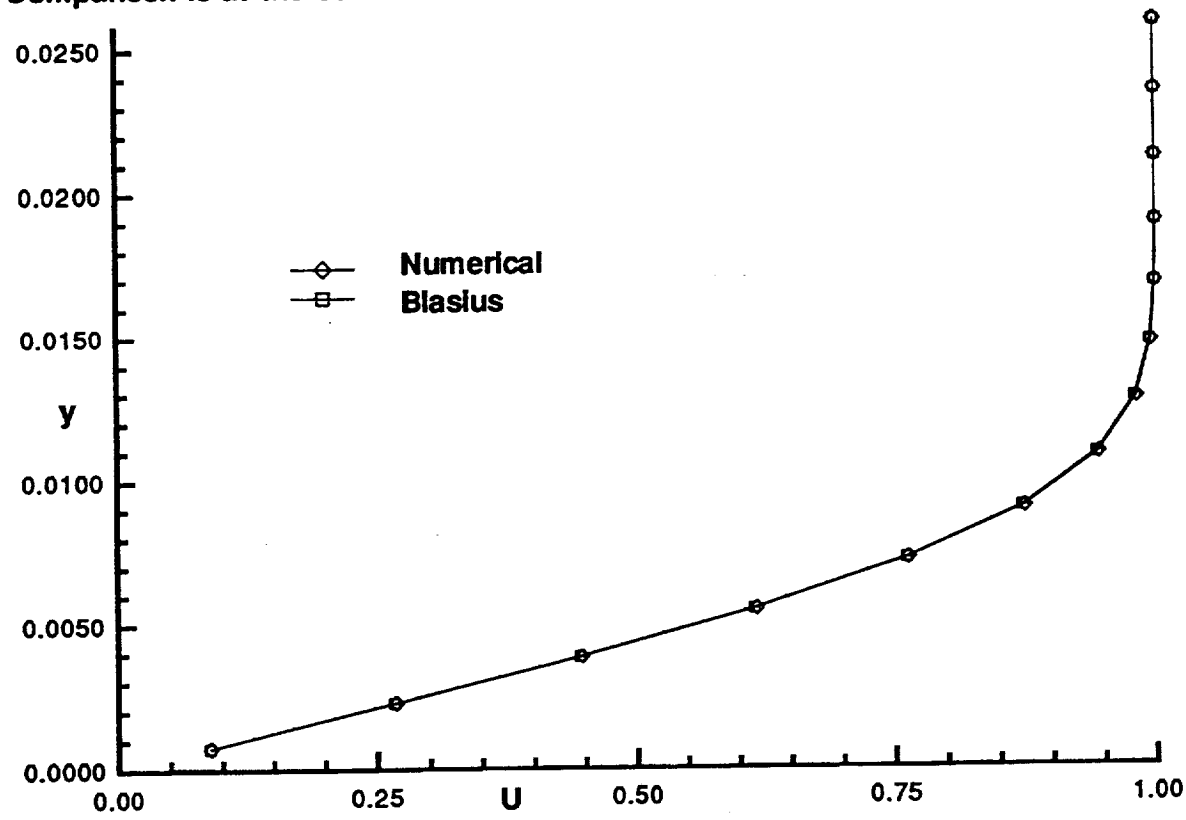


**Figure 10 d. Comparison of numerical results and Blasius solution at x = .816. Comparison is at the cell center of each solution element. 110 x 28 grid.**

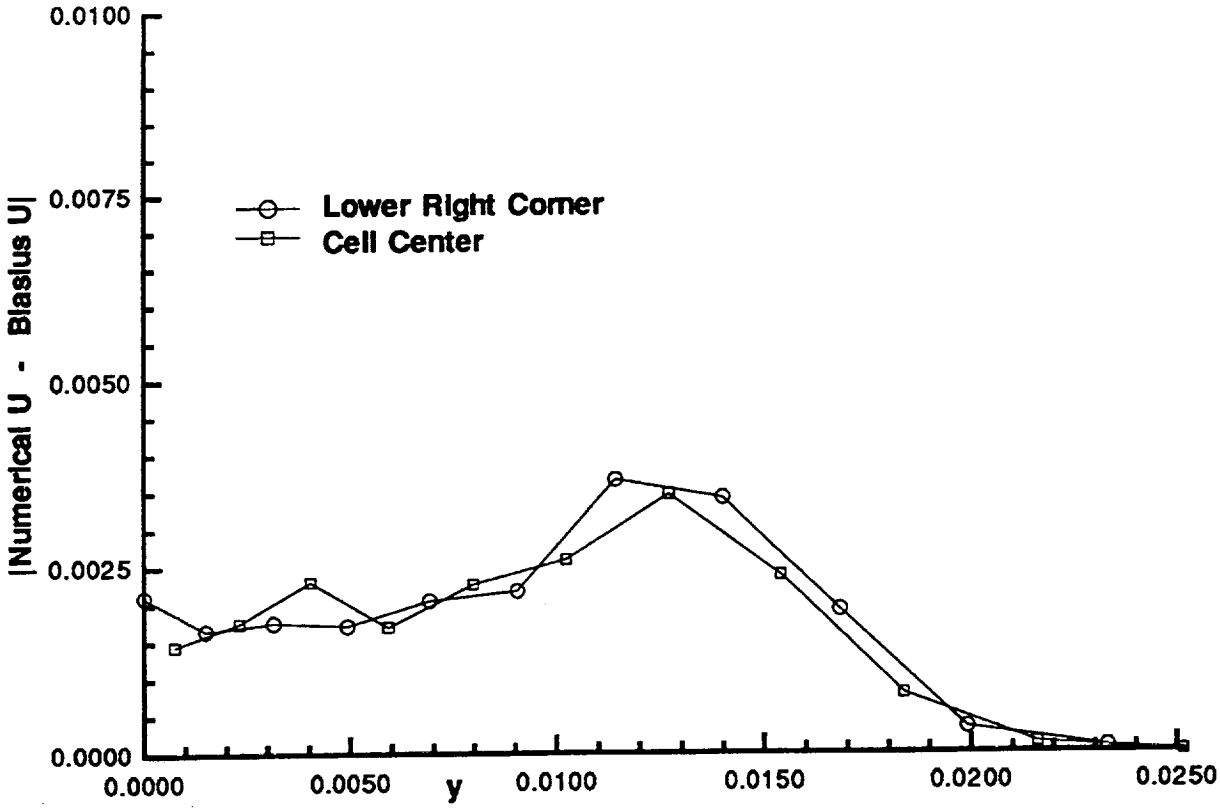


**Figure 10 e. Difference between discrete u velocity and Blasius solution at cell center and lower right corner of solution elements. x = .81, .82. 81 x 22 grid.**

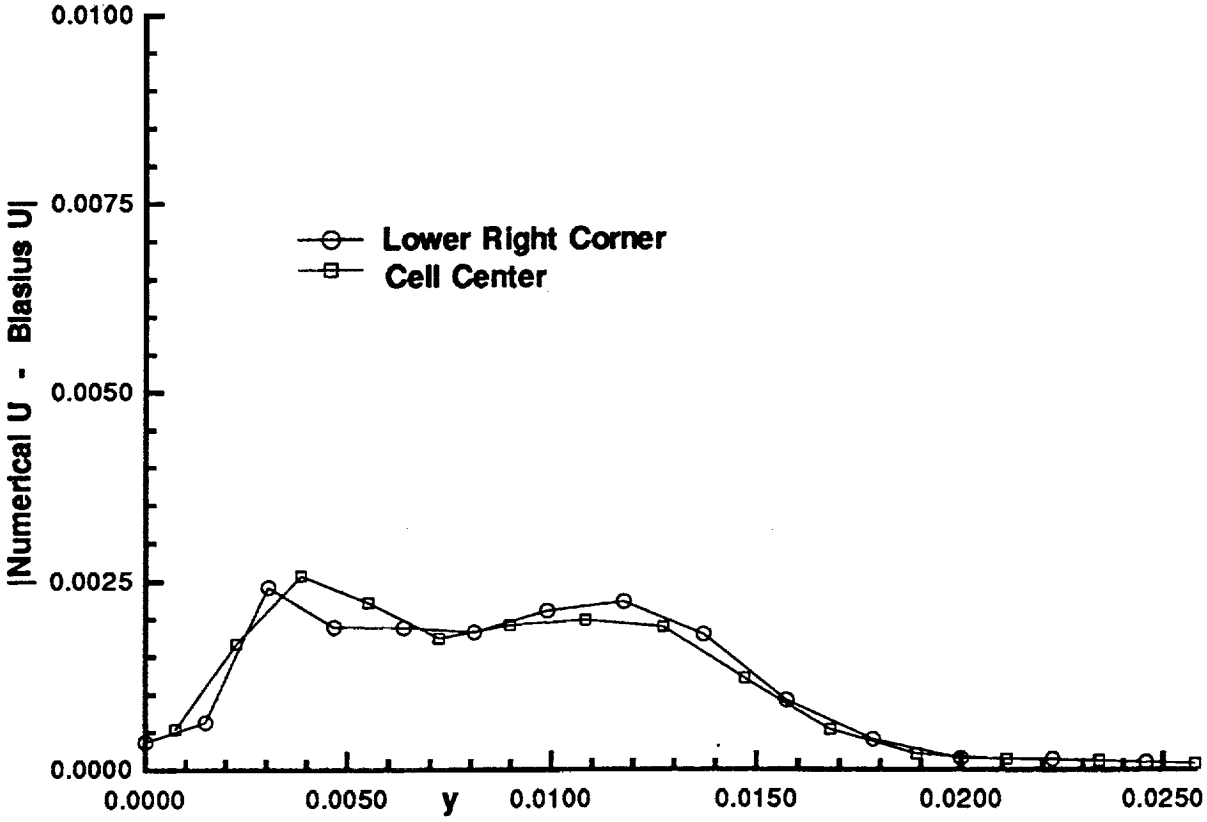


**Figure 10 f. Difference between discrete u velocity and Blasius solution at cell center and lower right corner of solution elements. x = .816, .822. 110 x 28 grid.**

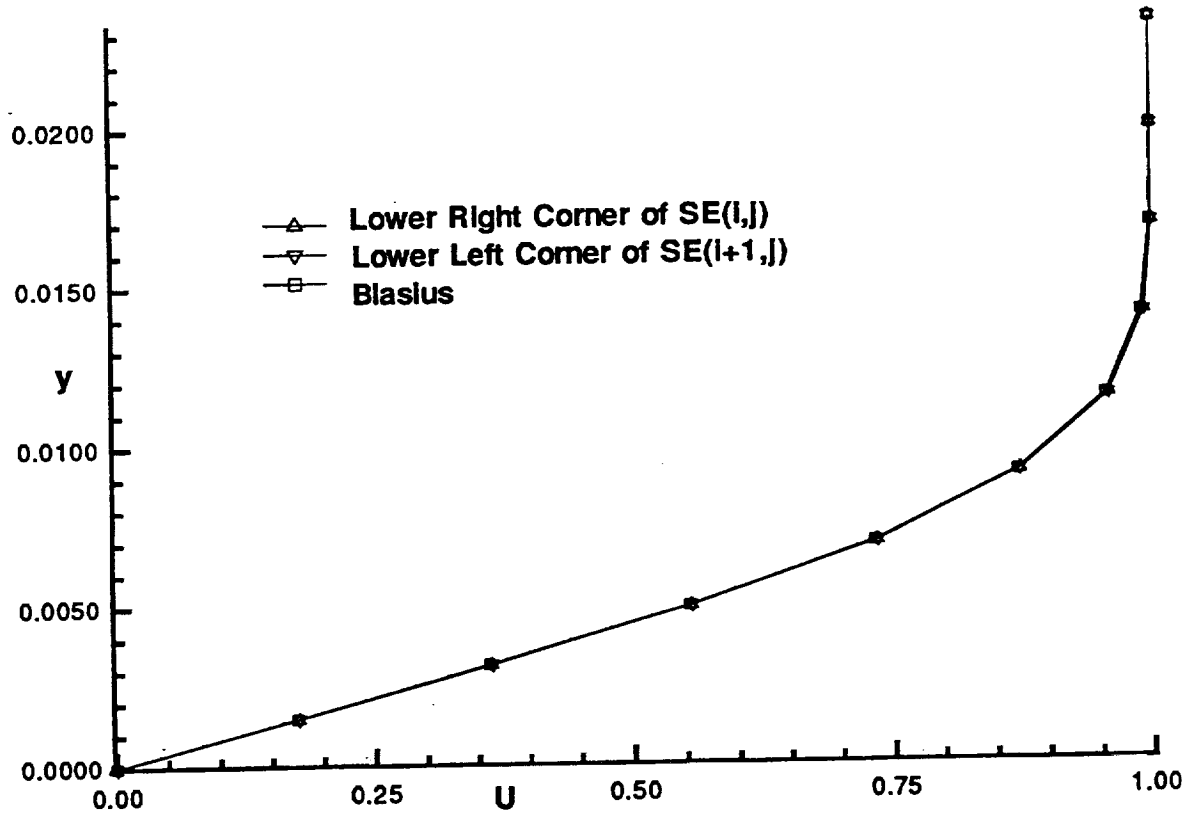


**Figure 10 g. Comparison of numerical results from adjacent solution elements and the Blasius solution. x = .82, 81 x 22 grid.**


**Figure 11 a. 81 x 22 computational grid with uniform x spacing. dxte = .02.**

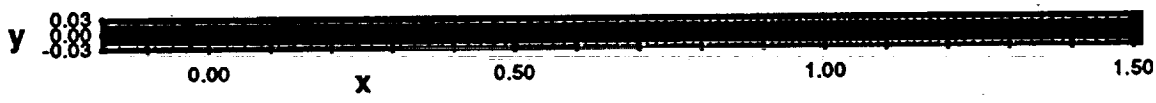


**Figure 11 b. 98 x 22 computational grid with 2% exponential x stretching. dxte = .01**

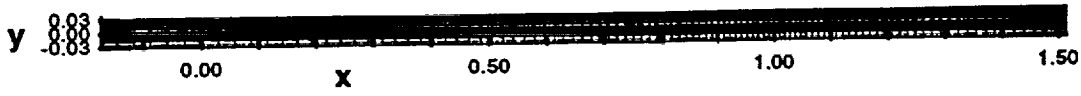


**Figure 11 c. 102 x 22 computational grid with 2.1% exponential x stretching. dxte = .009**

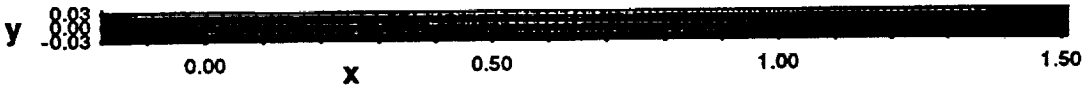


**Figure 11 d. 106 x 22 computational grid with 2.3% exponential x stretching. dxte = .008**

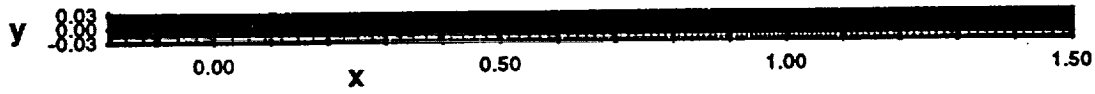


**Figure 11 e. 110 x 22 computational grid with 2.5% exponential x stretching. dxte = .007**

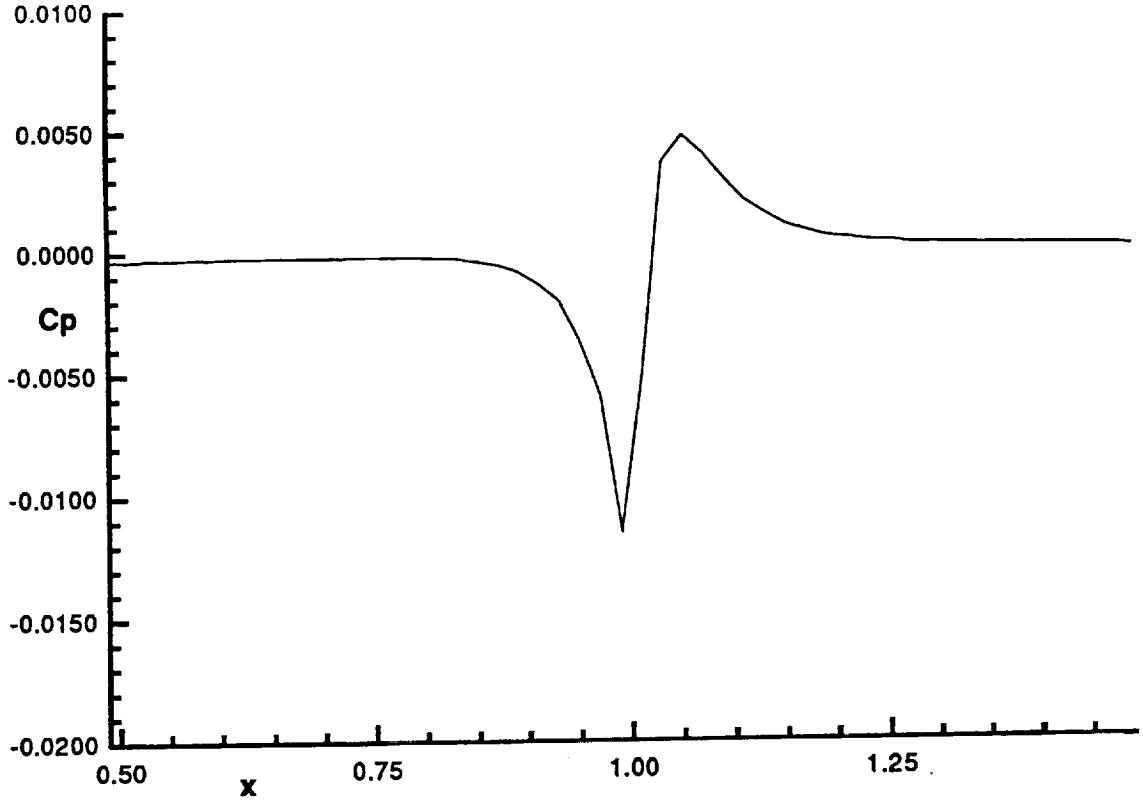


**Figure 12 a. Pressure coefficient in the trailing edge region. 81 x 22 grid.**

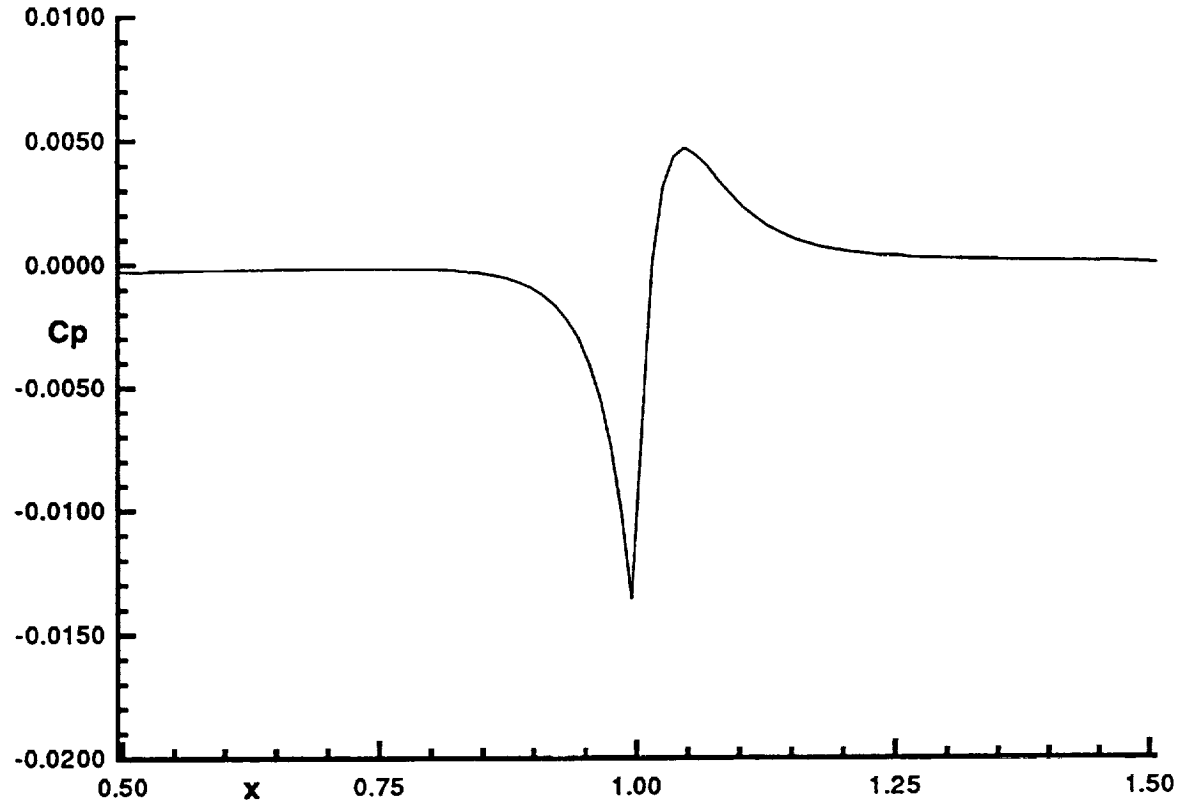


**Figure 12 b. Pressure coefficient in the trailing edge region. 98 x 22 grid.**

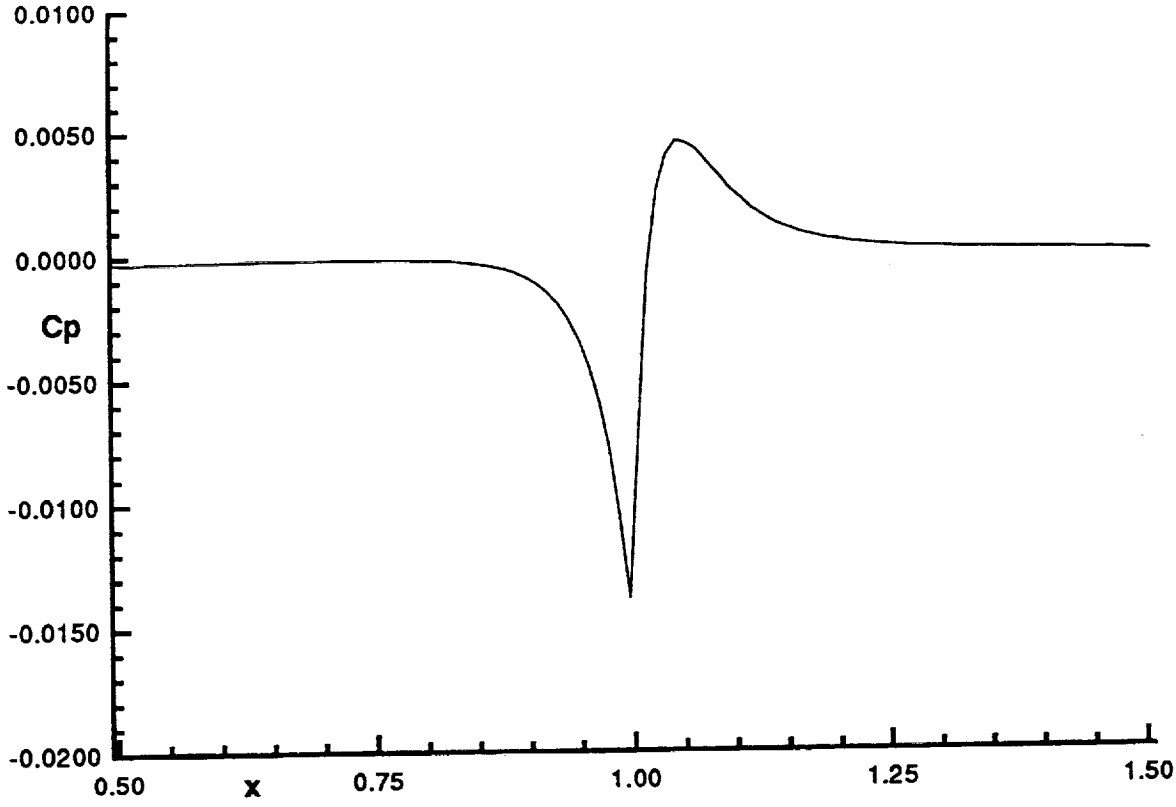


**Figure 12 c. Pressure coefficient in the trailing edge region. 102 x 22 grid.**

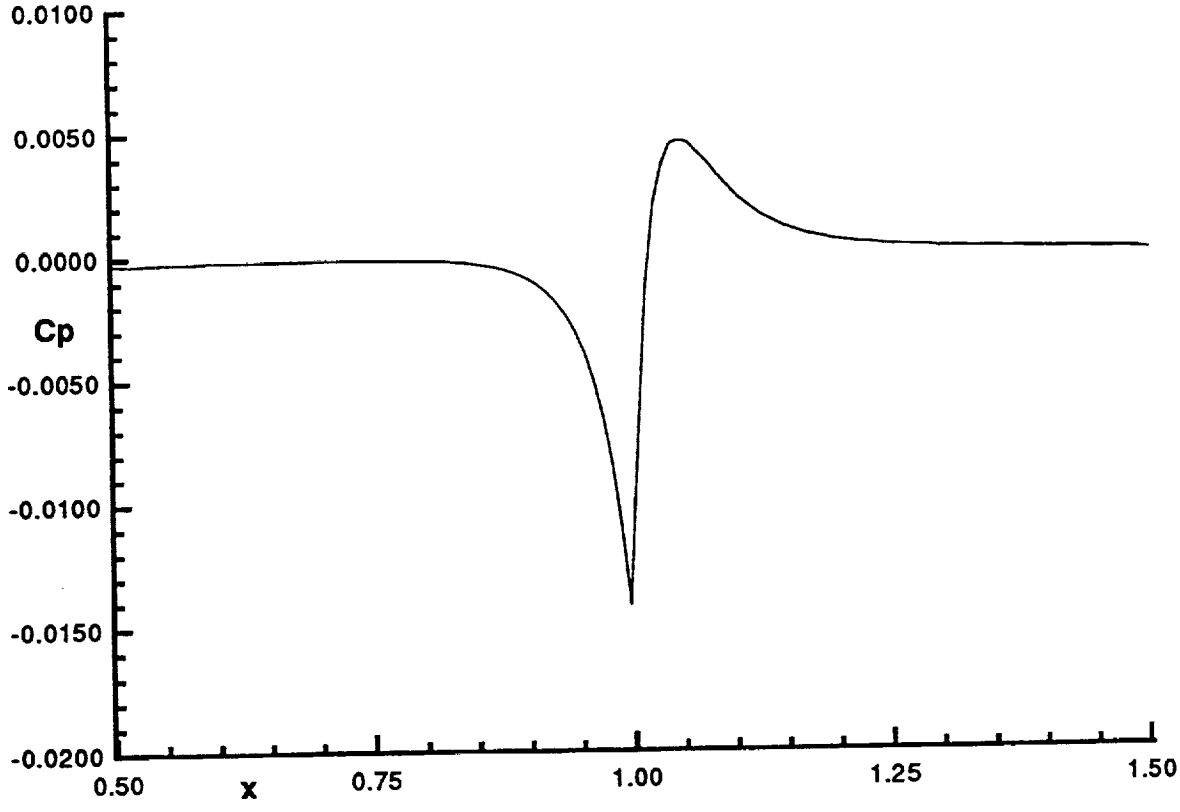


**Figure 12 d. Pressure coefficient in the trailing edge region. 106 x 22 grid.**

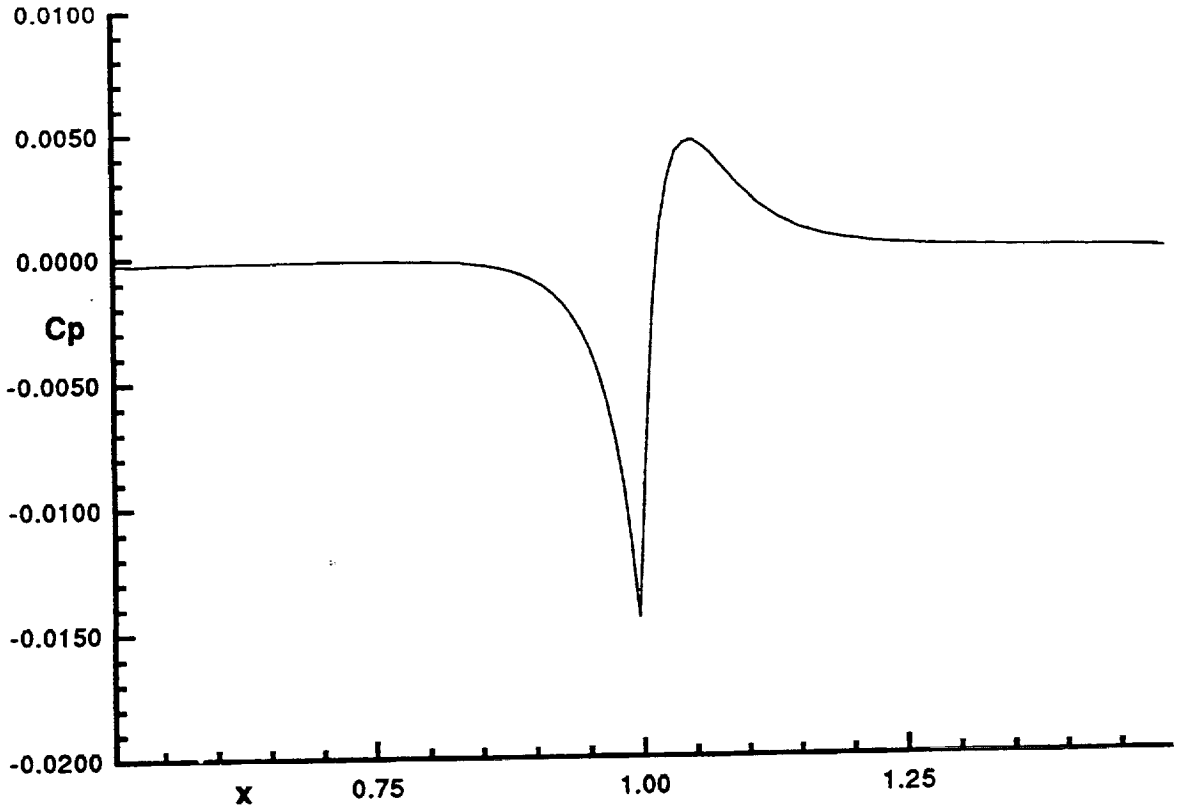


**Figure 12 e. Pressure coefficient in the trailing edge region. 110 x 22 grid.**

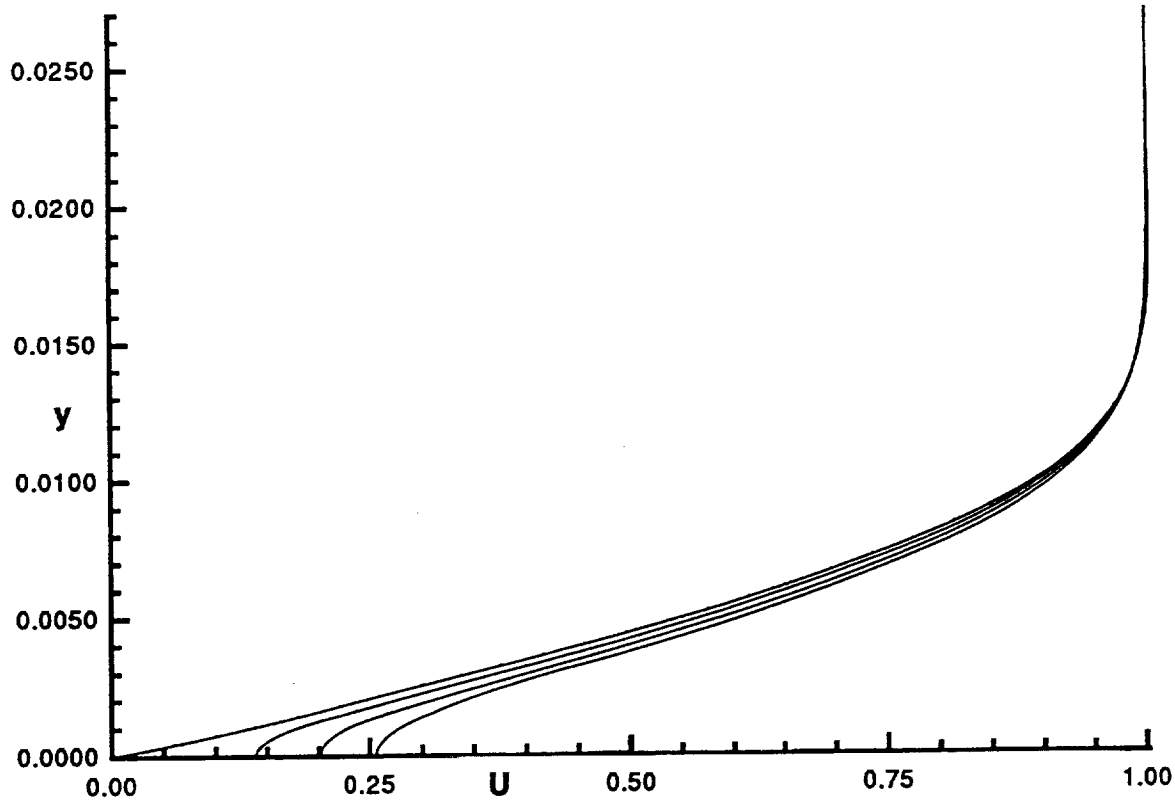


**Figure 13 a. Predicted streamwise velocity profile in the trailing edge region from an 81 x 22 grid with uniform x spacing. dxte = .02.**

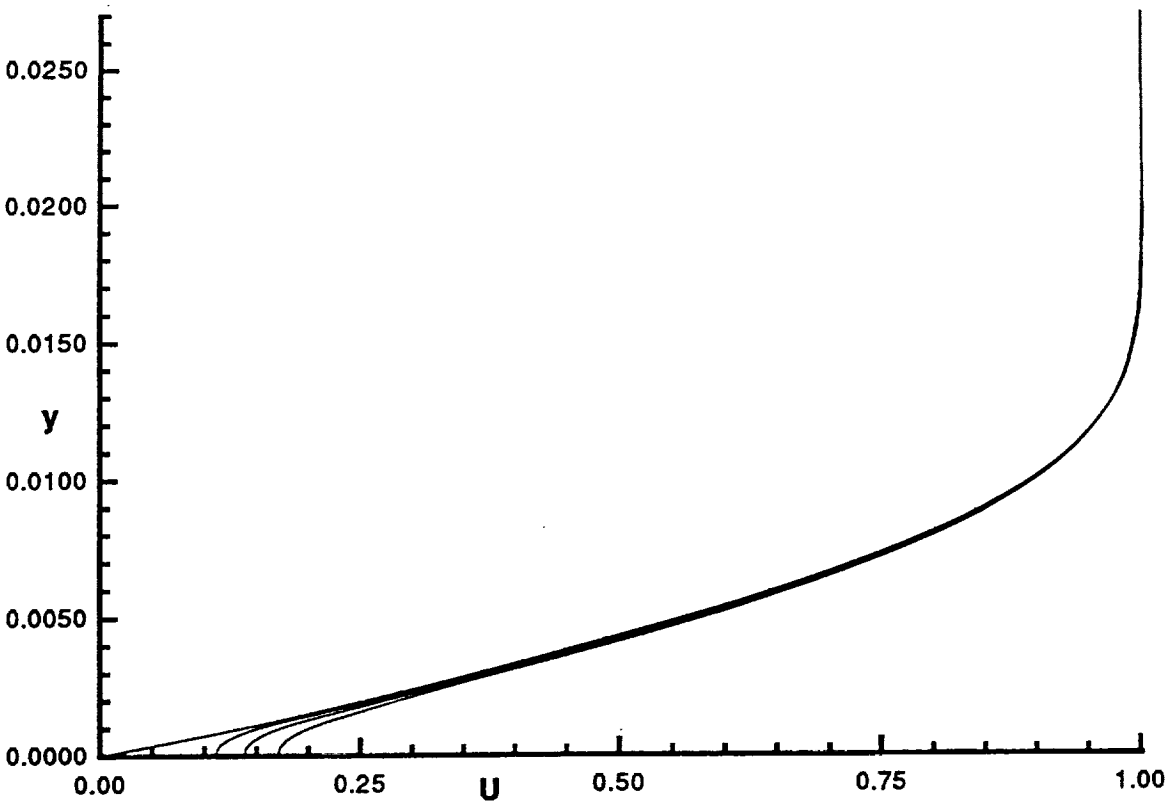


**Figure 13 b. Predicted streamwise velocity profile in the trailing edge region from a 110 x 22 grid with exponential x stretching. dxte = .007.**

# REPORT DOCUMENTATION PAGE

Form Approved
OMB No. 0704-0188



| 1. AGENCY USE ONLY (*Leave blank*) | 2. REPORT DATE | 3. REPORT TYPE AND DATES COVERED |
|---|---|---|
| | April 1994 | Technical Memorandum |

**4. TITLE AND SUBTITLE**

A New Flux-Conserving Numerical Scheme for the Steady, Incompressible Navier-Stokes Equations

**5. FUNDING NUMBERS**

WU-505-62-52

**6. AUTHOR(S)**

James R. Scott

**7. PERFORMING ORGANIZATION NAME(S) AND ADDRESS(ES)**

National Aeronautics and Space Administration
Lewis Research Center
Cleveland, Ohio 44135-3191

**8. PERFORMING ORGANIZATION REPORT NUMBER**

E-8642

**9. SPONSORING/MONITORING AGENCY NAME(S) AND ADDRESS(ES)**

National Aeronautics and Space Administration
Washington, D.C. 20546-0001

**10. SPONSORING/MONITORING AGENCY REPORT NUMBER**

NASA TM-106520

**11. SUPPLEMENTARY NOTES**

Responsible person, James R. Scott, organization code 2660, (216) 433-5863.

**12a. DISTRIBUTION/AVAILABILITY STATEMENT**

Unclassified - Unlimited
Subject Categories 02, 34, and 64

**12b. DISTRIBUTION CODE**

**13. ABSTRACT** (*Maximum 200 words*)

This paper is concerned with the further development of a new numerical method, the space-time solution element (STS) method, for solving conservation laws. The present work focuses on the two-dimensional, steady, incompressible Navier-Stokes equations. Using first an integral approach, and then a differential approach, the discrete flux conservation equations presented in a recent paper are re-derived. Here (i) a simpler method for determining the flux expressions at cell interfaces is given; (ii) a systematic and rigorous derivation of the conditions used to simulate the differential form of the governing conservation law(s) is provided; (iii) necessary and sufficient conditions for a discrete approximation to satisfy a conservation law in $E_2$ are derived; and (iv) an estimate of the local truncation error is given. A specific scheme is then constructed for the solution of the thin airfoil boundary layer problem. Numerical results are presented which demonstrate the ability of the scheme to accurately resolve the developing boundary layer and wake regions using grids which are much coarser than those employed by other numerical methods. It is shown that ten cells in the cross-stream direction are sufficient to accurately resolve the developing airfoil boundary layer.

**14. SUBJECT TERMS**

Navier-Stokes; Flux; Conservation law; Conservative; Boundary layer; Flat plate; Blasius; Steady; Incompressible; Space-time; Conservation element; Solution element; STS

**15. NUMBER OF PAGES**

49

**16. PRICE CODE**

A03

| 17. SECURITY CLASSIFICATION OF REPORT | 18. SECURITY CLASSIFICATION OF THIS PAGE | 19. SECURITY CLASSIFICATION OF ABSTRACT | 20. LIMITATION OF ABSTRACT |
|---|---|---|---|
| Unclassified | Unclassified | Unclassified | |